# Quantum Gates and Decoupling in Qubits with Fixed Transverse Coupling

by

Guiyang Han

A thesis
presented to the University of Waterloo
in fulfillment of the
thesis requirement for the degree of
Master of Science
in
Physics(Quantum Information)

Waterloo, Ontario, Canada, 2017

I hereby declare that I am the sole author of this thesis. This is a true copy of the thesis, including any required final revisions, as accepted by my examiners.

I understand that my thesis may be made electronically available to the public.

## Abstract

Among all the quantum computer candidates, the superconducting system is one of the most convincing platforms due to its strong couplings and scalability. To be more specific, this thesis focuses on the superconducting system, in which the artificial atoms are controlled longitudinally and coupled without any intermediate devices.

This thesis studies the implementation of universal quantum gates in the fixed-coupling longitudinal controlled superconducting systems. We will discuss the reasons of choosing this system and also address the difficulties towards one/two-qubit gates in the many-qubit system. Meanwhile, we will review the state-of-the-art achievements of implementing quantum gates in such a system.

We propose a superconducting decoupling method in this thesis. Firstly, we state that our algorithm can effectively 'turn off' arbitrary couplings. Then, we analyze the errors of our decoupling method and prove that the errors are ignorable when a sequence of decoupling gates are applied on non-nearest-neighboring qubits. We verify the efficiency of our decoupling method using the numerical simulations, which are well-matched with the theoretical predictions. The irrelevant coupling strengths are suppressed to the third order. Using 99.6% fidelity isolated CNOT and 99.89% single-qubit gates, we obtain a fidelity of 97.8% with the CNOT implementation in a five-qubit system over 14.84 ns.

The decoupling method is not limited to this specific system. The algorithm is derived in general and can be applied to other quantum systems which has a time-independent Hamiltonian. We expect this work will be useful for implementing universal quantum gates.

## Acknowledgements

## Dedication

This thesis is dedicated to my beloved Physics. Hope he realizes this tiny research and likes it. Also, I would like to delicate this thesis to my parents, but they do not speak English, other than the sentence 'Sorry, I do not speak English.'

# Table of Contents

# List of Tables

# List of Figures

# List of Abbreviations

**BCH** Baker-Campbell-Hausdorff 23–25, 32

**FLICFORQ** Fixed LInear Couplings between Fixed Off-Resonant Qubits 2

**GRAPE** GRadient Ascent Pulse Engineer 2, 61, 63

**NMR** Nuclear Magnetic Resonance 5, 21, 29, 63

**PDE** Partial Differential Equation 14, 16

**RF** Rotating Frame 5, 10, 11, 13, 16, 18, 19, 21, 25–27, 31, 38, 51, 54

**RWA** Rotating Wave Approximation 5, 11, 16, 20, 53

**SD** Selective Darkening 2, 15, 17, 20, 28

# Chapter 1

# Introduction

Quantum theory is a branch of physics that explains the nature and behavior of matter and energy on the atomic and subatomic level. Through many great discoveries over the last century, quantum theory successfully predicts a great number of properties that cannot be explained using classical theories.

Unlike the classical bit, a quantum bit (qubit) in superposition can be either state 0, 1 or any linear combination of them (superposition). In 1992, Deutsch and Jozsa showed that the property of superposition can be used to solve a black box problem with only one query whereas a classical computer requires at least $2^n$ queries[1] [3]. Later, in 1994, Peter Shor showed that with quantum bits, factoring could be solved in polynomial time [4]. There are many more examples that can be listed here that have proven quantum computers possess the ability to outperform classical computers.

Over the past few years, scientists have tried to build a quantum computer on different platforms([5], [6]). The superconducting system is one of the main candidates due to its scalability and potential to achieve fast operations. This thesis will introduce an algorithm engineered for a particular type of Hamiltonian, which could be a useful resource for developing a scalable superconducting quantum computer.

## 1.1   Scalable Superconducting System

Many types of constraints manifest themselves in all kinds of quantum systems, one of which involves handling a large number of qubits. According to DiVincenzo's criterion [7],

---

[1]$n$ is the number of total bits.

to build a quantum computer, a system needs to be able to carry out a set of universal gates. In a 1D-qubit array (one type of quantum computers), one possible universal set of gates consists of CNOT gates (on nearest qubits) and single-qubit gates, according to the Solovay-Kitaev theorem [8]. It has been proven that any CNOT gate needs a finite coupling strength. This indicates that the 1D-qubit array requires a method to introduce couplings between qubits that are involved with CNOT gates. However, these couplings disturb other gate implementations at the same time.

A general approach for superconducting systems towards building a quantum computer is to design a 1D-array with nearest couplings. Based on this approach, several designs are proposed to get rid of extra couplings when implementing a gate, such as tunable couplers and tunable energy splittings (details described in chapter 2), which try to 'turn off' some of the couplings by sacrificing lifetimes of the qubits. Both designs introduce extra equipment to the system. This approach makes quantum gates easy to implement, but the qubits' lifetime is greatly reduced [9], [10], [11]. The equipment also occupies a significant amount of space in the experimental setups.

Alternatively, there are algorithms to implement quantum gates without additional equipment. For example, Selective Darkening (SD) [12], Fixed LInear Couplings between Fixed Off-Resonant Qubits (FLICFORQ) [13] and Cross Resonance [14] are algorithms for the CNOT gate implementations. However, lack of compatibility with multi-qubit systems is one common problem among these algorithms.

The same scaling problem happens to pulse engineering techniques like GRadient Ascent Pulse Engineer (GRAPE) [15], which is a numerical optimization method to find the pulses that implement a certain gate. In principle, such a technique is able to produce high fidelity gates for any well-defined quantum system. However, similar to all other optimization problems, GRAPE needs to sample a great number of initial pulse sequences, and the sample size grows quadratically with the number of qubits in the system. There are solutions to this problem like the subsystem approach[16], but it is hard to argue that these solutions still hold for systems with strong coupling strengths and when there is a large number of qubits in the system. Meanwhile, in a fixed-coupling system, the number of elements we need to manipulate for a quantum gate is much larger than the number of parameters we can control. Such a mismatch of the freedoms makes GRAPE algorithm's performance questionable on a large number of qubits.

This thesis addresses the scaling problem by introducing a method called superconducting decoupling. Our method does not require extra equipment. It transforms the Hamiltonian of a fixed-coupling superconducting system into an effective Hamiltonian with arbitrary couplings. The decoupling method activates only the couplings that we desire,

which makes scalable quantum gates possible in fixed-coupling systems.

## 1.2   Outline of the Thesis

This thesis focuses on implementing quantum gates in fixed-coupling superconducting multi-qubit systems. It is a fundamental step in quantum computing towards building a quantum computer.

In chapter 2, I will first introduce the fundamental features of a quantum computer and then review the relative background of superconducting systems. I will also discuss the reasons for choosing the fixed-coupling design over others. At last, I will introduce some widely accepted methods to characterize the dynamics of a fixed-coupling system.

In chapter 3, I will introduce some previous works on implementing quantum gates. In this chapter only, we assume that there are no undesirable couplings. In the first section, I will introduce the single-qubit gate algorithm, which has been experimentally verified to have a 99.99% fidelity [17] [2]. Then, I will introduce Selective Darkening [18] as the method we choose to implement CNOT gates. Among all others, this method gives a comparable fidelity (around 99.99% from simulations) and a rather clear derivation with fewer estimations.

In chapter 4, I will focus on the fixed-coupled superconducting system under instantaneous gates. In this chapter, the only problem that I try to establish is how to 'turn off' (i.e. decouple) some couplings in a system. I will start by introducing the decoupling method in the lab frame Hamiltonian. Then, I will show that this lab frame decoupling method can be integrated into the rotating frame. All single-qubit operations discussed in this chapter are assumed to be 100% accurate and instantaneous.

In chapter 5, I will discuss two attempts for extending instantaneous single-qubit gates to pulse gates. As one can imagine, there is no such thing as instantaneous gates; any quantum gate is a summary of qubits' dynamics over a period of time. One approach towards making the gates discussed in chapter 4 into pulse gates is to use the control strengths relatively stronger than couplings in order to ignore them. However, what makes this approach less attractive is the errors scale with the number of qubits. Alternatively, the errors can be greatly avoided by applying slow single-qubit gates under some additional conditions.

---

[2]In fact, to achieve such a high fidelity, we also need error filters, which we would no cover in this thesis.

In chapter 6, I will provide some simulations done in Matlab. I achieved fidelities of 99.93% and 99.6% on the single-qubit gates and CNOT correspondingly when there were no extra couplings. With these gates, I simulated the CNOT gates in a three-qbuit system and achieved 96.0% fidelity(on average) and 93.0% in the five-qubit system.

# Chapter 2

# Theoretical Bases

In this chapter, I will cover some theoretical foundations of quantum dynamics. I will start by introducing the concept of qubits and gates in section 2.1, which are building blocks of quantum computers and bear an analogue to bits and gates in classical computers. In section 2.2, I will review several designs of superconducting quantum computers and briefly discuss the aspects of each system. In section 2.3, I will introduce a method called Rotating Frame (RF) [19], which is a useful tool for analyzing evolutions that consist of fast and slow oscillations. Section 2.4 presents an estimation method called Rotating Wave Approximation (RWA) [20], which has been adapted in many research fields and proven to work very well. In section 2.5, I will introduce the transition strength as one of the many ways to characterize a quantum system.

## 2.1   Quantum Computation

Just like (classical) computers in our daily life, quantum computers are expected to operate in similar ways. This indicates the need for well-defined quantum bits and gates. There are many candidates for the quantum computers. Any physical system with non-linear elements could be used to build a quantum bit (qubit), for example: Nuclear Magnetic Resonance (NMR) [5], ion traps [21], optical atoms [22], quantum dots [22] and Nitrogen-vacancy Center [23].

A qubit is characterized by a specific scenario in a carefully designed quantum system, which has well-defined states $|0\rangle$, and $|1\rangle$. As a superconducting qubit, state $|0\rangle$ corresponds to a circuit with the lowest energy and state $|1\rangle$ corresponds to the circuit with a higher

energy. Due to the presence of the magnetic field, energies (states) change continuously in time, which can be characterized by the system's Hamiltonian. A quantum gate is a summary of these evolutions over a certain period of time.

A qubit can be any linear combination of $|0\rangle$ and $|1\rangle$. It has the following expression:

$$|\psi\rangle = \alpha|0\rangle + \beta|1\rangle, \tag{2.1}$$

where $\alpha$ and $\beta$ are complex numbers.

The Dirac notation is a common way to describe states and operators to make them mathematically computable. In Dirac notation, states are represented by vectors:

$$|\psi\rangle = \begin{pmatrix} \alpha \\ \beta \end{pmatrix}. \tag{2.2}$$

Also the operators are represented by matrices. A set of operators in a vector space $V$ is called a basis if the operators are linearly independent and every operator in $V$ is a linear combination of this set. Many bases can be defined for a single vector space. In a 2-dimensional space, one famous basis is called Pauli matrices [24]:

$$X = \begin{pmatrix} 0 & 1 \\ 1 & 0 \end{pmatrix}, \qquad Y = \begin{pmatrix} 0 & -i \\ i & 0 \end{pmatrix}, \qquad Z = \begin{pmatrix} 1 & 0 \\ 0 & -1 \end{pmatrix} \quad \text{and} \quad I = \begin{pmatrix} 1 & 0 \\ 0 & 1 \end{pmatrix}. \tag{2.3}$$

For higher dimensional spaces, multi-qubit gates are necessary to form a basis. The Solovay-Kitaev theorem [8] states that any quantum gates can be decomposed into CNOT and two other single-qubit gates ($H$ and $T$ gates).



$$CNOT = \begin{pmatrix} 1 & 0 & 0 & 0 \\ 0 & 1 & 0 & 0 \\ 0 & 0 & 0 & 1 \\ 0 & 0 & 1 & 0 \end{pmatrix}$$

Figure 2.1: **CNOT gate representation.** The CNOT matrix representation (left) and its circuit representation (right).

A quantum system can be called a computer if it is capable of performing 'good' single-qubit gates and CNOT gates. The gates are created through various control methods

and they have a chance of failure. Fidelity is a metrics used to measure how well a gate is performed. Given two gates $U_1, U_2$ with the dimension $d \otimes d$, the fidelity $F$ [25] is calculated as:

$$F = \frac{1}{d^2}|\text{tr}(U_1^\dagger U_2)|, \tag{2.4}$$

where $0 \leq F \leq 1$ and $F = 1$ means operation $U_1$ behaves the same as $U_2$.

## 2.2 Superconducting Qubit

There are many approaches towards building the world first quantum computer. In the superconducting circuit approach, a qubit is constructed from electrical elements and some of them are microscopic. Actually, a persuasive design has not yet been devised. Various ways are proposed to construct qubits as well as coupling them.

There are three major types of qubits: charge, flux and phase qubit. [1]
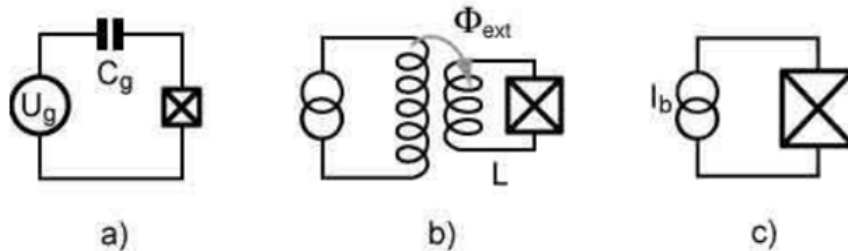


Figure 2.2: **Different types of superconducting qubits.** [1] a) Charge qubit; b) Flux qubit; c) Phase qubit (referred as prototypical models by Devoret.) Figure Courtesy: M. H. Devoret, et al.

After considering all three of the designs, we chose to analyze our algorithm on the flux qubits. First of all, a flux qubit has the largest nonlinearity among all three superconducting qubit types. This means the states $|0\rangle$ and $|1\rangle$ can be easily distinguished. Secondly, the dynamics of qubits are controlled by external applied fluxes. This control method is very convenient; their forms can be manipulated freely and can be precisely directed to any specific qubit in a multi-qubit system without too much noise.

The Hamiltonian of a single flux qubit in its degeneracy point[1] can be expressed as:

$$H_\triangle = \frac{\triangle}{2}Z + f(t)X, \tag{2.5}$$

where $X, Y$ are Pauli matrices; $f(t)$ is the external flux; $\triangle$ is the Zeeman frequency[2].

Coupling flux qubits can be done easily through allocating them near each other. The capacitances between the qubits will effectively connect them; however, due to the difficulties of analyzing the dynamics, scientists have tried different designs to overcome this issue.

As Devoret outlined in 2004 [1], there are three major ways to couple the qubits, which are all have been experimentally achieved at this point:

1. Zeeman frequencies for all qubits are the same and couplings can be turned on/off using intermediate devices. ([9], [10], [26]).

2. Couplings between qubits are fixed; Zeeman frequencies are tunable by having additional single-qubit control pulses(Xmon Qubit) ([27], [11], [28]).

3. Fixed-coupling and fixed Zeeman frequencies. ([12],[13], [29]).

|  |  | Zeeman Frequency | |
| --- | --- | --- | --- |
|  |  | Fix | Tunable |
| Coupling Frequency | Fix | Method 3 | Method 2 |
|  | Tunable | Method 1 | N/A |

Table 2.1: **Different multi-qubit designs in the superconducting system.** Predicted by Devoret, there are three major ways to couple the qubits. All of them have been experimentally achieved.

Method 1 and 2 employee extra device to the systems in order to deal with the unwanted couplings. However, they also cause the systems to decoherence (loss of the quantum information) very fast [1]. This thesis will focus on the third method, which we refer to as the fixed-coupling system. We state that our decoupling method has the potential to enable the CNOT gate implementations in the multi-qubit fixed-coupling system.

---

[1]Degeneracy point is a setup of qubit to make it has a long lifetime.
[2]A Zeeman term is the qubit's energy frequency gap; a Zeeman frequency is the coeifficient of the Zeeman term.

The Hamiltonian we are going to use throughout the thesis is constructed by flux qubits described in Eq. 2.5 with inductance couplings between the nearest qubits in an 1D-array[3]:

$$H(t) = H_\triangle + H_\text{J} + H_\text{d}(t).\tag{2.6}$$

Here, $H_\triangle$ is the Zeeman frequency; $H_\text{d}(t)$ is the single-qubit control. Both terms are not affected by whether the qubits in the system are coupled or not. $H_\text{J}$ is the extra Hamiltonian caused by coupling qubits capacitively. They can be expressed as the following:

$$H_\triangle = -\sum_i \frac{\triangle_i}{2} Z_i,\tag{2.7}$$

$$H_\text{d}(t) = \sum_i f_i(t) X_i\tag{2.8}$$

and

$$H_\text{J} = \sum_i J_{i,i+1} X_i X_{i+1}.\tag{2.9}$$

Here, the s $i$ is the qubit index; $\triangle_i$'s are Zeeman frequencies; $f_i(t)$'s are shapes of control pulses; $J_{i,i+1}$'s are coupling strengths. We ignore all couplings with a distance more than one qubit because they are exponentially weaker than the nearest couplings.

The decoupling method also works well in systems with superconducting qubits coupled by resonators. This system has the advantage of strong couplings between qubits that lead to fast quantum entangling gates. The system can be characterized by the famous Jaynes-Cummings Hamiltonian [30] :

$$H_\text{JC} = \hbar\omega(a^\dagger a + \frac{1}{2}) - \frac{\triangle}{2} Z + J(a^\dagger \sigma^- + a\sigma^+),\tag{2.10}$$

where $\omega$ is the qubit frequency and $a, a^\dagger, \sigma^-, \sigma^+$ are ladder operators.

The coupling terms specified in the equation is not exactly XX-coupling as Eq. 2.9. However, Jaynes-Cummings Hamiltonian gives the same expression as the fixed-coupling Hamiltonian in rotating frame. This means that they can be decoupled in the same way using the method we are going to introduce in this thesis.

---

[3]We will refer this structure as the 'fixed-coupling' system throughout the thesis.

## 2.3 Rotating Frame

When describing a system with the Hamiltonian, scientists try to avoid having terms significant larger than others. On one hand, large amplitude terms make the evolutions sensitive to time. In a laboratory environment, to measure a quantum system at a very specific time is challenging; if a evolution is not captured at the exact time, the extra evolution will cause a significant error. On the other hand, with the presence of large amplitude terms, the weak terms cannot be observed precisely.

Rotating frame is an useful technique for eliminating terms with large amplitudes in a Hamiltonian. Referring to the Hamiltonian in Eq. 2.6, it describes how states evolve in a laboratory environment, which is called the lab frame Hamiltonian. In this Hamiltonian, single-qubit Zeeman frequencies ($\triangle_i$) are few times larger than the controlling ($f_i(t)$) and coupling strengths ($J_{i,i+1}$). This is not a desirable property because qubits are dominated by the fast single-qubit (Zeeman) rotations, so that, other less trivial dynamics are significantly disturbed and result in less effective quantum gates.

The problem of large Zeeman frequencies can be solved by finding a suitable frame rotation. We consider a reference frame rotates at the same angular speed as the Zeeman terms.

For a state $|\psi(t)\rangle$ evolving under the Hamiltonian $H(t)$ (in lab frame), we define another state $|\psi(t)\rangle_{RF}$ which has a time-dependent relation to the original state [4]:

$$|\psi(t)\rangle_{\mathrm{RF}} = e^{iH_\triangle t}|\psi(t)\rangle. \tag{2.11}$$

In the next step, we use the Schrödinger's time-dependent equation to find the Hamiltonian for the state $|\psi(t)\rangle_{RF}$:

$$H_{\mathrm{RF}}(t)|\psi(t)\rangle_{\mathrm{RF}} = i\frac{d}{dt}|\psi(t)\rangle_{\mathrm{RF}}. \tag{2.12}$$

For the right-hand-side of the equation, we express state in the lab frame, do the derivative and then change the state back to the RF:

$$i\frac{d}{dt}|\psi(t)\rangle_{\mathrm{RF}} = -H_\triangle e^{iH_\triangle t}|\psi(t)\rangle + ie^{iH_\triangle t}\frac{d}{dt}|\psi(t)\rangle \tag{2.13}$$

$$= -H_\triangle|\psi(t)\rangle_{\mathrm{RF}} + e^{iH_\triangle t}H_{\mathrm{LF}}e^{-iH_\triangle t}|\psi(t)\rangle_{\mathrm{RF}} \tag{2.14}$$

---

[4]Plank unit is used here for clarity, where $c = \hbar = 1$.

By expanding $H_{\mathrm{LF}}$ using Eq. 2.6 and the operator commutative property $[e^{-iH_\triangle t}, H_\triangle] = 0$, we get the on-resonance rotating frame Hamiltonian Eq. 2.11, which is:

$$H_{\mathrm{RF}}(t) = e^{iH_\triangle t}(H_{\mathrm{J}} + H_{\mathrm{d}}(t))e^{-iH_\triangle t}. \tag{2.15}$$

We observe that all the terms in the RF Hamiltonian are small in amplitudes. Instead, they have periodical behaviors caused by the frame rotation.

In this section, we have seen a particular type of the frame transformation. It is easy to extend this method of frame rotation to other rotations. By replacing $e^{iH_\triangle t}$ in Eq.2.11 with any unitary $U(t)$, the Hamiltonian of the corresponding rotating frame can be found. Note that an exponentiation form of $U(t)$ with time-independent coefficients is highly preferred, because its time-derivative does not introduce extra terms in the RF Hamiltonian.

## 2.4  Rotating Wave Approximation

RWA is a common tool in quantum dynamic analysis [31]. It states that when a Hamiltonian is periodic, its fast oscillating (short period) terms can be ignored as long as their amplitudes are not large.

Despite how unreliable it might sound, this approximation performs quite well in many practical situations and is widely accepted in quantum dynamics. In this section, I will present a theoretical proof.

**Statement:**

Let $H(t)$ denotes the Hamiltonian, and $U(t_0, t)$ denotes the evolution of the system from $t_0$ to $t$. Rotating Wave Approximation (RWA) states that the evolution can be predicted quite precisely with only the slow oscillating terms in $H(t)$.

**Proof:**

The evolution $U(t_0, t)$ can be expanded using the Dyson series [32] in terms of $H(t)$, which is:

$$U(t_0, t) = 1 - i\int_{t_0}^{t} dt_1 H(t_1) - \int_{t_0}^{t} dt_2 H(t_2) \int_{t_0}^{t_2} dt_1 H(t_1) + i\int\int\int ... \tag{2.16}$$

11

Since most of the Hamiltonians we are interested in are periodic, the integrals are proportional to their frequencies $\omega$ as:

$$\int e^{i\omega t} dt = \frac{e^{i\omega t}}{i\omega}.$$
(2.17)

The amplitude of the numerator is always one regardless of the frequency $\omega$, but a large $\omega$ value in the denominator makes the equation to have a small value. Therefore, only the low frequency terms are significant in a Hamiltonian.

A nature question would be how to determine whether a frequency is considered insignificant than others. For the estimation that we are going to use in this thesis:

$$H_{\mathrm{d}}(t) = a\cos(\omega t)X = \frac{a}{2}(e^{i\omega t} + e^{-i\omega t})X = \frac{a}{2}e^{i\omega t}(1 + e^{-2i\omega t})X \approx \frac{a}{2}e^{\pm i\omega t}X,$$
(2.18)

where '$\pm$' depends on the direction of static Hamiltonian $H_0$.

The above estimation is quite accurate, since the frequency $\omega$ is always going to be on-resonance. Since the bandwidth of the system will be around the resonant frequency, the off-resonance term is very far away from the bandwidth that is safe to be ignored.

## 2.5 Time Evolution of Hamiltonian

As we all know, an efficient way to characterize a system is to use the Hamiltonian. However, there are no obvious ways to derive the evolution operator from a Hamiltonian. According to the Schrödinger equation:

$$i\frac{d}{dt}|\psi(t)\rangle = H(t)|\psi(t)\rangle,$$
(2.19)

if the Hamiltonian $H(t)$ is time-independent, the solution is simply as the following:

$$|\psi(t)\rangle = e^{-iHt}|\psi(0)\rangle.$$
(2.20)

When the Hamiltonian is time-dependent, there is no universal solution so far. Some of the time-dependent Hamiltonians are even not solvable. Fig. 2.3 lists several approaches as an example. In this section, to serve the purpose of finding the qubits' dynamics, I will introduce a specific approach. Some people may refer this approach as the transition strength between states. Later, we will use this technique to find the control parameters for single and two-qubit gates.

12
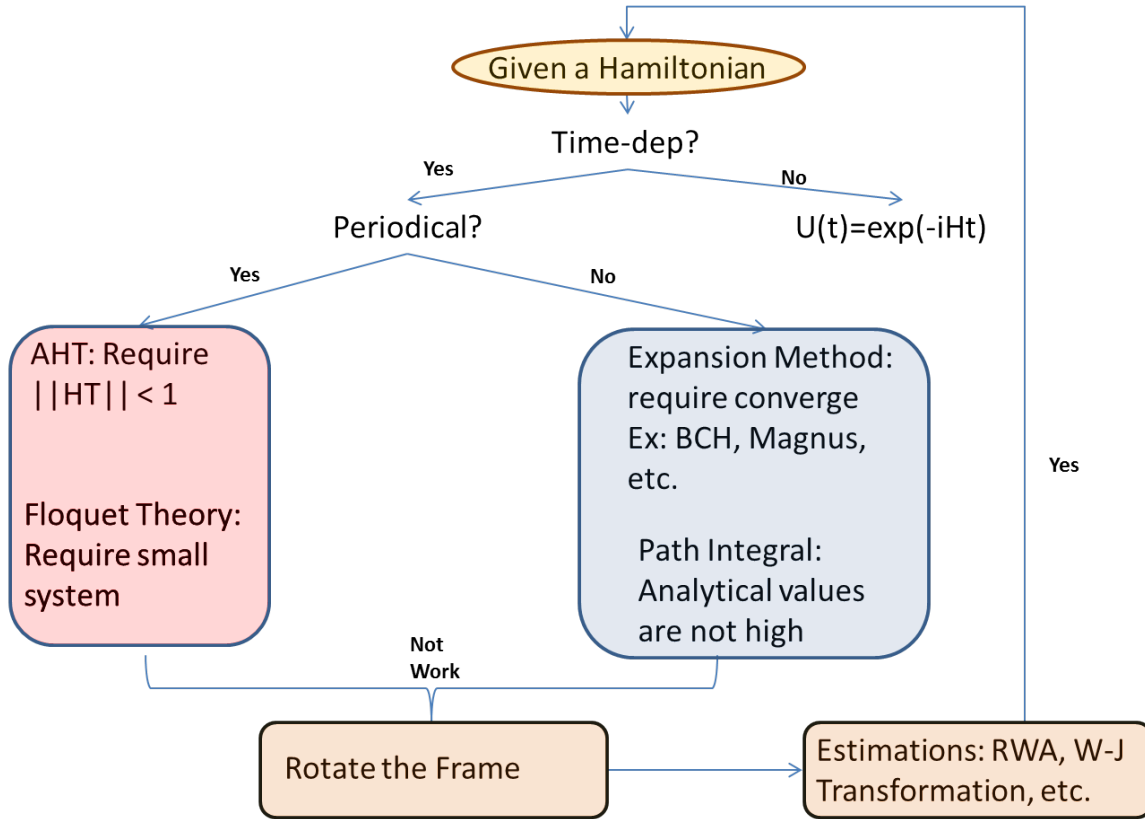
Figure 2.3: **A non-exhaustive flow chart of ways to solve a Hamiltonian.** It describes several available ways towards getting the evolution matrix from a Hamiltonian. The approaches may vary depending on the properties of a Hamiltonian.

**Transition strength:** [31]

Starting from the Schrödinger's picture[5], which is:

$$i\frac{d}{dt}|\psi(t)\rangle_{\mathrm{RF}} = H_{\mathrm{RF}}(t)|\psi(t)\rangle_{\mathrm{RF}}. \tag{2.21}$$

We define the state $|\psi(t)\rangle_{\mathrm{RF}}$ as a linear combination of time-independent basis vectors $\{|v_i\rangle\}_i$:

---

[5]We use RF Hamiltonian for convenience.

$$i\frac{d}{dt}\sum_n c_n(t)|v_n\rangle = H_{\text{RF}}(t)\sum_n c_n(t)|v_n\rangle. \tag{2.22}$$

Then, we can multiply $\langle v_a|$ on the both sides:

$$i\langle v_a|\sum_n \dot{c}_n(t)|v_n\rangle = \langle v_a|H_{\text{RF}}(t)\sum_n c_n(t)|v_n\rangle. \tag{2.23}$$

This gives an expression for each of the time-dependent coefficient $c_a(t)$:

$$i\dot{c}_a(t) = \sum_n c_n(t)\langle v_a|H_{\text{RF}}(t)|v_n\rangle, \qquad \text{for all the possible } c_a(t). \tag{2.24}$$

Here, $\langle v_a|H_{\text{RF}}(t)|v_n\rangle$ is referred as the transition strength between the state $|v_a\rangle$ and $|v_n\rangle$; $c_a, c_n$ are the corresponding probability coefficients.

Usually $c_a(t)$'s cannot be solved due to the complexity of Partial Differential Equation (PDE). However, if we have enough controls over these transition strengths, we can manufacture the equations to be solvable.

# Chapter 3

# Controlled Dynamics of Fixed-Coupling Qubits

Over the years, researchers were trying to build a quantum computer with different systems. The language of 'gate' and 'qubit' has been adapted in general [33]. Among all the landscapes of quantum computers, 2D surface code stands out because of simplicity and scalability. It has been proven that the gates in a surface code needs to have fidelities higher than 99.9% [34]. In the current stage of superconducting systems this fidelity can be achieved, but we are facing a trade-off between the fidelity and coherence time as stated in section 2.2. It is not clear that which design is better or what degrees of the trade-off we want. The fixed-coupling system we discussed in this thesis has the advantage of a long coherent time, but the transverse couplings make the Hamiltonian difficult to solve.

In this chapter, I will present the previous works for implementing one-qubit and CNOT gates in the fixed-coupling system. In section 3.1, I will introduce the algorithm for implementing single-qubit gates. In section 3.2, I will introduce Selective Darkening (SD), which is an algorithm for CNOT gates in the fixed-coupling system. It achieves a 99.99% fidelity according to the simulation [12], where the threshold of surface codes is well satisfied.

## 3.1 Single-Qubit Gate

We will consider a single-qubit Hamiltonian[1] of the form:

$$H(t) = -\frac{\triangle}{2} Z + a \cos(\omega t + \phi(t)) X, \tag{3.1}$$

where $\omega$, $a$ [2] and $\phi(t)$ are the control frequency, amplitude and phase correspondingly.

To have a low noise experimentally, the control amplitude $a$ is generally set to few times smaller than the Zeeman frequency $\triangle$. The difference between frequencies is a good clue of using rotating frame (RF). We rotate the lab frame with the operator $e^{-i\frac{\triangle}{2}Zt}$:

$$H_{\mathrm{RF}}(t) = a e^{-i\frac{\triangle}{2}Zt} \cos(\omega t + \phi) X e^{i\frac{\triangle}{2}Zt} = H_+ + H_-, \tag{3.2}$$

where $H_+$, $H_-$ are clockwise and anticlockwise rotations defined as:

$$H_\pm = a e^{-i\frac{\triangle}{2}Zt} e^{\pm i(\omega t + \phi)} X e^{i\frac{\triangle}{2}Zt} \tag{3.3}$$

$$= (a e^{\pm i\phi}) e^{-i\frac{\triangle}{2}Zt} e^{\pm i\omega t} X e^{i\frac{\triangle}{2}Zt}. \tag{3.4}$$

Once we figure out the Hamiltonian in RF, we can calculate the transition strengths:

$$\langle 0|H_+ + H_-|1\rangle \approx \langle 0|H_+|1\rangle = a e^{+i\phi} \langle 0|e^{-i\frac{\triangle}{2}Zt} e^{+i\omega t} X e^{i\frac{\triangle}{2}Zt}|1\rangle = a e^{+i\phi} e^{-i(\triangle-\omega)t} \tag{3.5}$$

and

$$\langle 1|H_+ + H_-|0\rangle \approx \langle 1|H_-|0\rangle = a e^{-i\phi} \langle 1|e^{-i\frac{\triangle}{2}Zt} e^{-i\omega t} X e^{i\frac{\triangle}{2}Zt}|0\rangle = a e^{-i\phi} e^{+i(\triangle-\omega)t}. \tag{3.6}$$

Rotating Wave Approximation (RWA) is being used in Eq. 3.5 to ignore $H_-$ because it is the faster term compared to $H_+$. Similarly, we ignore $H_+$ in Eq. 3.6.

Note that choosing $\omega = \triangle$ is the only way to avoid the system from rotating 'too fast'. Then by solving the partial differential equation (PDE) with an initial state, we can have a complete description of the system[3]:

$$c_0(t) = e^{i\phi} \cos(at) \tag{3.7}$$

and

$$c_1(t) = e^{-i\phi} \sin(at). \tag{3.8}$$

Fig. 3.1 shows that with a proper control, the initial state periodically changes between $|0\rangle$ and $|1\rangle$.

---

[1]In both this section and the next, undesired couplings are not considered. Discussions on many-coupling systems will take place in both Chapter 3 and 4.

[2]Generally speaking, we can have a time-depedent $a$, but here we only take it as the constant.

[3]I use the ground state as the initial state for example
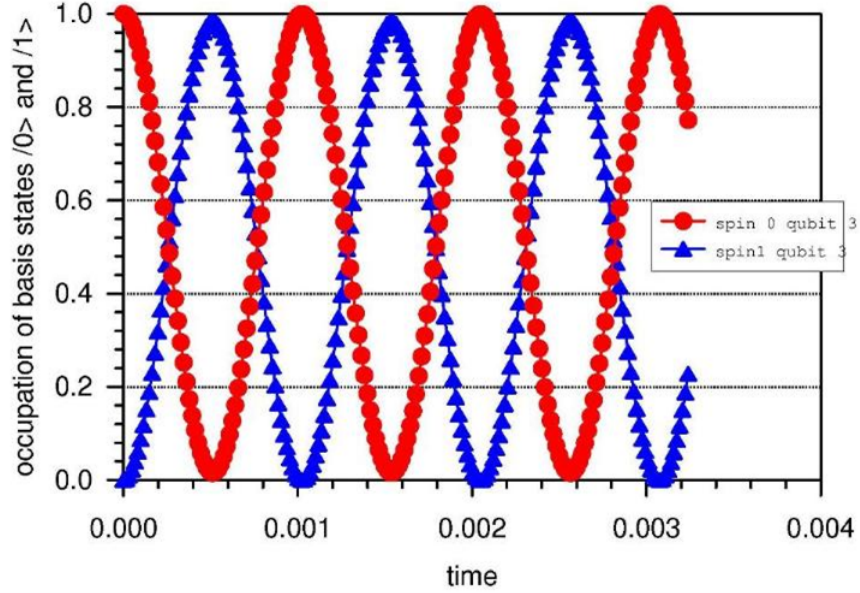
Figure 3.1: **Rabi oscillation of a single qubit.** [2] A state is initiated as $|0\rangle$. The probability of observing a state is plotted against time. With the matched control frequency, the state oscillates between being observed as $|0\rangle$ and $|1\rangle$. Figure Courtesy: R. P. Feynman, et.al

## 3.2   CNOT–Selective Darkening

This section gives a simple overview of Selective Darkening (SD). It is a method to implement CNOT in a fixed-coupling system. Details can be found in Groot's paper. [18]

In a two-qubit system, the lab frame Hamiltonian is defined as:

$$H = H_0 + H_J + H_d(t), \tag{3.9}$$

$$H_\triangle = -\frac{\triangle_1}{2}Z_1 - \frac{\triangle_2}{2}Z_2, \tag{3.10}$$

$$H_J = J_{12}X_1X_2 \tag{3.11}$$

and

$$H_d(t) = a_1\cos(\omega_1 t + \phi_1)X_1 + a_2\cos(\omega_2 t + \phi_2)X_2. \tag{3.12}$$

The control $H_d(t)$ is done through the magnetic flux, which can be made sufficiently flexible.

However, it is a convention to define $H_{\mathrm{d}}(t)$ in the above form because it captures both the phase and frequency of the control pulses.

As we discussed in earlier sections, it is never a bad idea to find the system's dynamics by transforming the Hamiltonian into RF:

$$H_{\mathrm{RF}}(t) = e^{i(H_\triangle + H_{\mathrm{J}})t} H_{\mathrm{d}}(t) e^{-i(H_\triangle + H_{\mathrm{J}})t}. \tag{3.13}$$

Here, we define our logic basis as the eigenstates of $H_\triangle + H_{\mathrm{J}}$. Note that the eigenstates are entangled in tensor product space and cannot be prepared or measured precisely. Luckily, for $J_{12} << |\triangle_1 - \triangle_2|$, these entangled states are nearly indistinguishable from tensor product states.

Expression of the eigenstates using tensor vectors as the followings:

$$|\tilde{0}\rangle = (\cos\theta_1; 0; 0; -\sin\theta_1), \tag{3.14}$$
$$|\tilde{1}\rangle = (0; \cos\theta_2; -\sin\theta_2; 0), \tag{3.15}$$
$$|\tilde{2}\rangle = (0; \sin\theta_2; \cos\theta_2; 0) \tag{3.16}$$

and

$$|\tilde{3}\rangle = (\sin\theta_1; 0; 0; \cos\theta_1), \tag{3.17}$$

where

$$\theta_1 = \frac{1}{2}\arctan(\frac{2J_{12}}{\triangle_1 + \triangle_2}) \tag{3.18}$$

and

$$\theta_2 = \frac{1}{2}\arctan(\frac{2J_{12}}{\triangle_1 - \triangle_2}). \tag{3.19}$$

By defining the states in the eigenbasis of $H_\triangle + H_{\mathrm{J}}$, state transitions maintain the same structure as the no coupling system. The blue/red arrows in Fig. 3.2 indicate that the connected states can evolve into one another. Without change the basis, the coupling $J_{12}$ introduces two extra transitions (red arrows). These transitions are captured by the entangled basis and the structure is the same as the no coupling case.
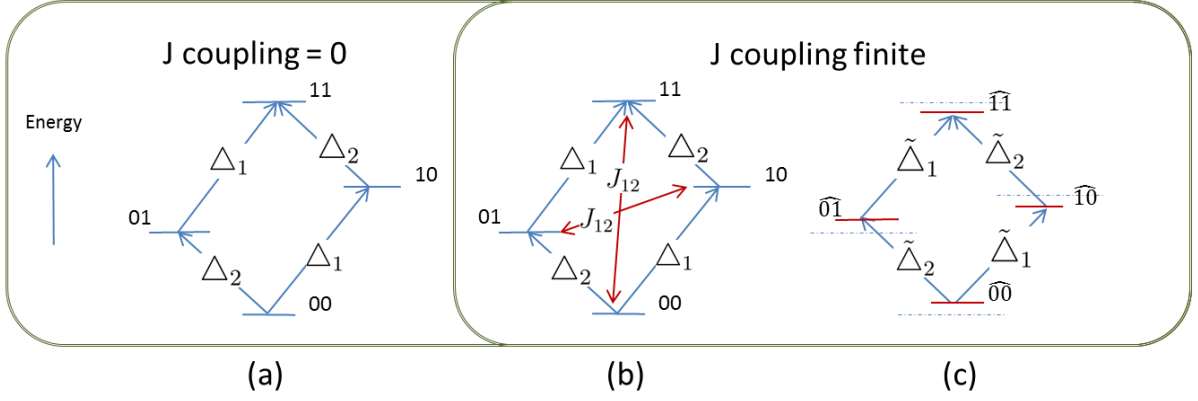
Figure 3.2: **Energy levels of two qubits with/without transverse couplings.** 00, 01, 10, 11 are eigenstates of the system without couplings; $\hat{0}0, \hat{0}1, \hat{1}0, \hat{1}1$ are the eigenstates of a finite coupling $J_{12}$. The altitude of each bar is a visual representation of the energy which a state possesses. $\triangle$'s and $\tilde{\triangle}$'s are the transition strengths. Arrows indicate the connected states are evolving into each other simultaneously under the corresponding Hamiltonian. In a) we see there are four transitions in the system with no coupling between two qubits. In b) we see that using the same states as before, the coupling introduces two extra transitions, which makes the evolution very hard to characterize. In c), by changing the basis, the number of transitions are reduced to four again.

A CNOT gate is an evolution that exchanges states $|10\rangle$ and $|11\rangle$. If we apply a pulse at frequency $\triangle_2$ in the system, it will only activate two transitions $|\tilde{1}0\rangle \leftrightarrow |\tilde{1}1\rangle$ and $|\tilde{0}0\rangle \leftrightarrow |\tilde{0}1\rangle$. However, it takes quite an effort to turn off $|\tilde{0}0\rangle \leftrightarrow |\tilde{0}1\rangle$ among two transitions, since they are activated by the same control frequency value. It turns out that a specific ratio between two qubits' control amplitudes can make it work.

To rewrite the above explanation as mathematical equations, we start from the RF Hamiltonian in Eq. 3.13 and an arbitrary state expressed in entangled basis:

$$H_{\mathrm{RF}}(t) = e^{i(H_\triangle + H_J)t} H_{\mathrm{d}}(t) e^{-i(H_\triangle + H_J)t}, \tag{3.20}$$

$$|\psi(t)\rangle_{\mathrm{RF}} = c_0(t)|\tilde{0}0\rangle + c_1(t)|\tilde{0}1\rangle + c_2(t)|\tilde{1}0\rangle + c_3(t)|\tilde{1}1\rangle, \tag{3.21}$$

where

$$H_{\mathrm{d}}(t) = a_1 \cos(\omega_1 t + \phi_1) X_1 + a_2 \cos(\omega_2 t + \phi_2) X_2. \tag{3.22}$$

Then, we can match the control frequencies $\omega_1, \omega_2$ to the entangled states after rotating

the frame:

$$\omega_1 = \omega_2 = E_3 - E_1 = \frac{1}{2}(\sqrt{4J^2 + (\triangle_1 + \triangle_2)^2} + \sqrt{4J^2 + (\triangle_1 - \triangle_2)^2}). \tag{3.23}$$

As a result, we only have the following transition strength expressions, since others are forbidden due to the mismatch of the frequencies [18]:

$$\langle \tilde{2}|H_{\mathrm{d}}(t)|\tilde{0}\rangle = +\frac{a_1}{2}e^{i\psi_1}\cos(\theta_1 + \theta_2) + \frac{a_2}{2}e^{i\psi_2}\sin(\theta_2 - \theta_1) \tag{3.24}$$

and

$$\langle \tilde{3}|H_{\mathrm{d}}(t)|\tilde{1}\rangle = +\frac{a_1}{2}e^{i\psi_1}\cos(\theta_1 + \theta_2) - \frac{a_2}{2}e^{i\psi_2}\sin(\theta_2 - \theta_1). \tag{3.25}$$

Lastly, we engineer the ratio of $a_1, a_2$ to make $\langle \tilde{2}|H_{\mathrm{d}}(t)|\tilde{0}\rangle = 0$, which is:

$$\frac{a_1}{a_2} = \frac{J_{12}}{\triangle_1 - \triangle_2}. \tag{3.26}$$

To sum up, this section briefly introduces SD. It operates on an entangled basis and uses it to carry out the CNOT gate with only the errors caused by RWA.

# Chapter 4

# Instantaneous Decoupling

The idea of decoupling originated from Nuclear Magnetic Resonance (NMR). It is a technique for making some/all terms in a Hamiltonian effectively zero (referred as being 'decoupled') [35] [36]. This idea is highly practical in NMR because the single-qubit gates, which the decoupling method heavily relied on, can be implemented very fast compared to the disturbance caused by the couplings.

In superconducting systems, it is possible to have large qubit-qubit couplings. This large coupling is favoured due to the possibility to implement fast coupling gates. However, in this case, the strength of the control pulses may not be much larger than the couplings, making the analysis of coupling difficult. Moreover, we are interested here in the couplings which are transverse with respect to the Zeeman terms, which further complicates the implementation of decoupling.

In this chapter, I will discuss the 'ideal' decoupling method in the 1D-array with fixed-couplings. All the single-qubit gates are assumed to have 100% fidelities and are instantaneous. In general, this assumption is too good to be true. However, the analysis will lead to the actual implementations which will be discussed in the next chapter and we will see that the pulse gates are the natural extensions to these instantaneous ones.

Fully and partially decoupling methods with the lab frame Hamiltonian are introduced in section 4.1 and 4.2 respectively; In section 4.3, I will introduce the decoupling method in the rotating frame (RF) by establishing the relations between a lab frame and its rotating frame.

## 4.1 Refocusing in the Lab Frame

In this section, we will see that how the refocusing (fully decoupled) method works in our fixed-coupling system. It is a method that creates an identity operation in a quantum system over any period of time. As mentioned above, in this chapter including all sections, we will assume the driving Hamiltonian $H_{\mathrm{d}}(t) = 0$. This makes the lab frame Hamiltonian of the fixed-coupling system time-independent.

A time-independent Hamiltonian (for example Eq. 2.6) generates a fixed consistent evolution in the system. Suppose that in this system, we are able to do instantaneous gates $G$ and $G^{\dagger}$. They are computed in a way that by applying $G$ and $G^{\dagger}$ at the beginning and the end of a period of the evolution can effectively change the basis of the Hamiltonian of this period. The new basis can be constructed in a way that the evolution on this basis negates the evolution of the original basis. So that, by having a sequence of a period of the evolution, gate $G$, the evolution of the same period and gate $G^{\dagger}$ our effective evolution is just identity because the evolution of the second period negates the first period.

For any time-independent Hamiltonian $H$, the time evolution operator from $t_0$ to $t$ can be expressed as an exponential form:

$$U(t_0, t) = e^{-iH(t-t_0)}. \tag{4.1}$$

Assuming that we are able to apply operators $G^{\dagger}$ and $G$ before and after the evolution of the system, which gives:

$$GU(t_0, t)G^{\dagger} = Ge^{-iH(t-t_0)}G^{\dagger}. \tag{4.2}$$

For the operators that are unitary:

$$G^{\dagger}G = I, \tag{4.3}$$

we can insert any number of $G^{\dagger}G$ pairs to Eq.4.2 and 'lift them up':

$$Ge^{iH(t-t_0)}G^{\dagger} = G(\sum_{a=0}^{\infty} \frac{-iH(t-t_0))^a}{a!})G^{\dagger} \tag{4.4}$$

$$= \sum_{a=0}^{\infty} \frac{i^a(t-t_0)^a}{a!}(GH^aG^{\dagger}) \tag{4.5}$$

$$= \sum_{a=0}^{\infty} \frac{i^a(t-t_0)^a}{a!}(GHG^{\dagger})^a \tag{4.6}$$

$$= e^{iGHG^{\dagger}(t-t_0)}. \tag{4.7}$$

Now, we assume that the operators $G$ and $G^\dagger$ satisfies:

$$GHG^\dagger = -H. \tag{4.8}$$

Then over a time interval $T$, the system can be refocused by the following gate sequence:

$$e^{\frac{1}{2}iHT}Ge^{\frac{1}{2}iHT}G^\dagger = e^{\frac{1}{2}iHT}e^{\frac{1}{2}iGHG^\dagger T} \tag{4.9}$$

$$= e^{\frac{1}{2}iHT}e^{-\frac{1}{2}iHT} \tag{4.10}$$

$$= I. \tag{4.11}$$

This result indicates that if we could find a pulse $G$ that satisfies Eq. 4.8, then by applying it twice the system can be refocused.

For the fixed-coupling Hamiltonian (two qubits) [18]:

$$H_0 = -\frac{\triangle_1}{2}Z_1 - \frac{\triangle_2}{2}Z_2 + J_{12}X_1X_2, \tag{4.12}$$

one possible refocusing pulse $G$ could be[1]:

$$G = X_1Y_2. \tag{4.13}$$

## 4.2 Decoupling in the Lab Frame

In this section, I will introduce decoupling, which is an extension of refocusing. Rather than 'erasing' the entire Hamiltonian, decoupling only 'erase' a part of the Hamiltonian.

The method of decoupling uses the same idea of refocusing outlined in Eq. 4.9, and also utilizes another result called Baker-Campbell-Hausdorff (BCH) lemma[2] [37]. It states that the matrix exponents of two multiplying exponentiations can be summed up with errors of second order and higher in the matrix norms.

**BCH Lemma:**

For any two operators $A$, $B$ and a constant $t$,

$$\begin{aligned}e^{iAt}e^{iBt} &= e^{i(A+B)t - [A,B]\frac{t^2}{2} - i([A,[A,B]]+[B,[B,A]])\frac{t^3}{12}\cdots} \\ &= e^{i(A+B)t} + O(t^2).\end{aligned} \tag{4.14}$$

---

[1]Some other decoupling gates are $Y_1X_2$, $Z_1Y_2$ and $X_1Z_2$.

[2]Sometimes, this also called CBH lemma. They are the same thing with different name orders.

In our situation, all the matrices are operators with norm one. As long as $t$ is small, we can estimate the evolutions with only the first order[3] in $t$. Using the BCH lemma, terms in $A$ and $B$ with the same expressions but different signs will get canceled. Perhaps an example of lab frame decoupling is more explanatory and this will be used for later chapters anyways.

The Hamiltonian of a three-qubit system (without external controls) is:

$$H_0 = -\frac{\triangle_1}{2}Z_1 - \frac{\triangle_2}{2}Z_2 - \frac{\triangle_3}{2}Z_3 + J_{12}X_1X_2 + J_{23}X_2X_3, \tag{4.15}$$

where the evolution over time $T$ under this Hamiltonian is:

$$e^{-iH_0T} = e^{-iH_0\frac{T}{2}}e^{-iH_0\frac{T}{2}}. \tag{4.16}$$

If we use a modified $G$ from Eq. 4.13 as the decoupling pulse:

$$G = Y_1, \tag{4.17}$$

Then, the 'sandwiched' evolution has the following Hamiltonian:

$$H_{0-} = GH_0G = Y_1(-\frac{\triangle_1}{2}Z_1 - \frac{\triangle_2}{2}Z_2 - \frac{\triangle_3}{2}Z_3 + J_{12}X_1X_2 + J_{23}X_2X_3)Y_1 \tag{4.18}$$

$$= +\frac{\triangle_1}{2}Z_1 - \frac{\triangle_2}{2}Z_2 - \frac{\triangle_3}{2}Z_3 - J_{12}X_1X_2 + J_{23}X_2X_3. \tag{4.19}$$

One possible sequence for decoupling qubit 1 is to apply the gate $G$ every $\delta t$ time:

$$Ge^{-iH_0\delta t}Ge^{-iH_0\delta t}Ge^{-iH_0\delta t}Ge^{-iH_0\delta t}... \tag{4.20}$$

$$= e^{-iH_{0-}\delta t}e^{-iH_0\delta t}e^{-iH_{0-}\delta t}e^{-iH_0\delta t}... \tag{4.21}$$

$$= e^{-i(H_0+H_{-0})\delta t}e^{-i(H_0+H_{0-})\delta t}... + N \times O(\delta t^2) \tag{4.22}$$

$$= e^{-\frac{i}{2}(H_0+H_{0-})t} + N \times O(\delta t^2) \tag{4.23}$$

$$= e^{-i(-\frac{\triangle_2}{2}Z_2-\frac{\triangle_3}{2}Z_3+J_{23}X_2X_3)t} + N \times O(\delta t^2). \tag{4.24}$$

As a result of the computations, we can see that the decoupling sequence with $G$ gates can simplify a three-qubit Hamiltonian to a two-qubit Hamiltonian. We say that the first qubit is 'decoupled' from the three-qubit system. The error here is $N \times O(\delta t^2)$ due to the

---

[3]In fact, in our error analysis, we considered second order errors as well. Here, we stick to the first order for simplicity.

BCH estimation, where $N = T/\delta t$. $O(\delta t^2)$ is the estimation errors for each time step $\delta t$, and it cumulates $N$ times.[4]

In general, the decoupling method is able to cancel an arbitrary subset of the coupling terms from the Hamiltonian. However, there are some further conditions we need to discuss, as well as the scalable implementation which will be covered in subsection 5.5.2.

## 4.3 Refocusing and Decoupling in Rotating Frame

Maybe there is a confusion about why we keep talking about the rotating frame if everything seems to work fine in the lab frame. In fact, the rotating frame is quite favored by experimentalists. In the rotating frame (RF), fast oscillations of the state are absent, facilitating a simpler description of the dynamics. After calculating the dynamics in the rotating frame, a translation back to the lab frame is necessary to calculate the system state. However, if the measurements applied to the system commute with the frame rotations, one can consider their action in the rotating frame.

In this section, I will introduce a method that establishes the relation between the lab and rotating frames. Then we can use this method to do decoupling in the rotating frame Hamiltonians.

We write the Hamiltonian of the fixed-coupling 1D-array in the lab frame as:

$$H_{\mathrm{LF}} = H_\triangle + H_{\mathrm{J}}, \tag{4.25}$$

where

$$H_\triangle = -\sum \frac{\triangle_i}{2} Z_i \tag{4.26}$$

and

$$H_{\mathrm{J}} = \sum J_{i,i+1} X_i X_{i+1}. \tag{4.27}$$

Then if we define the frame rotation $U_{ROT}(t)$ as :

$$U_{\mathrm{ROT}}(t) = e^{iH_\triangle t}, \tag{4.28}$$

_____
[4]This algorithm is only valid when $G$ is (close to) an instantaneous gate and the $\delta t$ is small.

this gives the RF state:

$$|\psi(t)\rangle_{\mathrm{RF}} = U_{\mathrm{ROT}}(t)|\psi(t)\rangle, \tag{4.29}$$

which leads to the RF Hamiltonian $H_{\mathrm{RF}}(t)$:

$$H_{\mathrm{RF}}(t) = U_{\mathrm{ROT}}(t)H_{\mathrm{J}}U_{\mathrm{ROT}}^{\dagger}(t). \tag{4.30}$$

We also know by Eq. 4.29, there is a clear relation between the evolutions under each of the Hamiltonians from an arbitrary time $t$ to $t + \triangle t$:

$$U_{\mathrm{LF}}(t, t + \triangle t) = U_{\mathrm{ROT}}^{\dagger}(t + \triangle t)U_{\mathrm{RF}}(t, t + \triangle t)U_{\mathrm{ROT}}(t), \tag{4.31}$$

where $U_{\mathrm{LF}}(t, t + \triangle t)$ indicates the evolution under the lab frame Hamiltonian from time $t$ to $t + \triangle t$. This could be proven by equating the states at different times. First we can use Eq. 4.29 to establish the relation at time $t$:

$$|\psi(t)\rangle_{\mathrm{LF}} = U_{\mathrm{ROT}}^{\dagger}(t)|\psi(t)\rangle_{\mathrm{RF}}. \tag{4.32}$$

Then, we can evolve both sides and they also hold the relation:

$$U_{\mathrm{LF}}(t, t + \triangle t)|\psi(t)\rangle_{\mathrm{LF}} = U_{\mathrm{ROT}}^{\dagger}(t + \triangle t)U_{\mathrm{RF}}(t, t + \triangle t)|\psi(t)\rangle_{\mathrm{RF}}. \tag{4.33}$$

Also, the states at time $t + \triangle t$ should also hold Eq. 4.29, which is:

$$|\psi(t + \triangle t)\rangle_{\mathrm{LF}} = U_{\mathrm{ROT}}^{\dagger}(t + \triangle t)|\psi(t + \triangle t)\rangle_{\mathrm{RF}} \tag{4.34}$$

$$= U_{\mathrm{ROT}}^{\dagger}(t + \triangle t)U_{\mathrm{RF}}(t, t + \triangle t)U_{\mathrm{ROT}}(t)|\psi(t)\rangle_{\mathrm{RF}}. \tag{4.35}$$

By equating Eq. 4.33 and Eq. 4.35, we can get the relation stated in Eq. 4.31:

$$U_{\mathrm{LF}}(t, t + \triangle t) = U_{\mathrm{ROT}}^{\dagger}(t + \triangle t)U_{\mathrm{RF}}(t, t + \triangle t)U_{\mathrm{ROT}}(t). \tag{4.36}$$

Eq. 4.31 is very important to our analysis. Using this equation, the rotating frame decoupling scheme can be implemented in three steps:

1. We find the decoupling gate $G$ in the lab frame to achieve the desired evolution $U_{\mathrm{D}}$, which is:

$$U_{\mathrm{D}} = ...GU_{\mathrm{LF}}(2\tau, 3\tau)GU_{\mathrm{LF}}(\tau, 2\tau)GU_{\mathrm{LF}}(0, \tau), \tag{4.37}$$

where $\tau$ is a small time interval.

2. Assuming that there is a decoupling sequence in the rotating frame with gates $\tilde{G}(t)$ that can achieve the desired evolution in the RF $\tilde{U}_{\mathrm{D}}$, which is:

$$\tilde{U}_{\mathrm{D}} = ...\tilde{G}(t)U_{\mathrm{RF}}(2\tau, 3\tau)\tilde{G}(t)U_{\mathrm{RF}}(\tau, 2\tau)\tilde{G}(t)U_{\mathrm{RF}}(0, \tau). \tag{4.38}$$

3. We transform $U_{\mathrm{RF}}$ to $U_{\mathrm{LF}}$ and find out what is the $\tilde{G}(t)$ that satisfies the equation:

$$...\tilde{G}(t)U_{\mathrm{RF}}(\tau, 2\tau)\tilde{G}(t)U_{\mathrm{RF}}(0, \tau) \tag{4.39}$$

$$= ...\tilde{G}(t)[U_{\mathrm{ROT}}(2\tau)U_{\mathrm{LF}}(\tau, 2\tau)U_{\mathrm{ROT}}^{\dagger}(\tau)]\tilde{G}(t)[U_{\mathrm{ROT}}(\tau)U_{\mathrm{LF}}(0, \tau)] \tag{4.40}$$

$$= ...\tilde{G}(t)U_{\mathrm{ROT}}(2\tau)]U_{\mathrm{LF}}(\tau, 2\tau)[U_{\mathrm{ROT}}^{\dagger}(\tau)\tilde{G}(t)U_{\mathrm{ROT}}(\tau)]U_{\mathrm{LF}}(0, \tau). \tag{4.41}$$

4. Equating Eq. 4.37 and Eq. 4.41 gives the expression of $\tilde{G}_n$, which is:

$$\tilde{G}_n = U_{\mathrm{ROT}}(n\tau)GU_{\mathrm{ROT}}^{\dagger}(n\tau), \tag{4.42}$$

Since we verified $Y$ pulses can be used for lab frame decoupling, the corresponding RF pulse is:

$$\tilde{G}_n = e^{iH_{\triangle}n\tau}\left(\sum_p Y_p\right)e^{-iH_{\triangle}n\tau} = \sum_p \cos(\triangle_p n\tau)Y_p - \sin(\triangle_p n\tau)X_p, \tag{4.43}$$

where the sum is over the indices $p$ corresponding to the qubits where the decoupling gates are applied, that have the Zeeman frequencies $\triangle_p$ and Pauli matrices $Y_p$, $X_p$.

Note that our decoupling gates in the lab frame is single-qubit operations, as well as the frame rotation. As a result, the decoupling gates in the rotating frame, which we will discuss later, must be single-qubit gates.

It is sufficient for us to use the Pauli-X and Y gates to decouple a 1D-qubit array as we mentioned. However, for the completeness of the discussion, a fully-coupled system can also be decoupled with a similar idea. Prior work [35] [36] found methods to arrange the evolutions according to combinatorial properties of the Hadamard matrices. So that, any arbitrary subset of the couplings in the fully-coupled system can be effectively decoupled.

# Chapter 5

# Superconducting Decoupling

In the previous chapter, we established that if single-qubit (decoupling) gates can be applied instantaneously, the couplings of a Hamiltonian can be manipulated with nearly no errors. However, all the gates in any quantum system are accomplished by evolving the system according to the Hamiltonian, the duration of a gate is unavoidably finite. This means that we need to do the decoupling gates with pulses, as well as other gates in the system.

Quantum operations do not always commute. Applying two implementations of gate at the same time can introduce extra evolution caused by non-commutativity. One good example would be the Selective Darkening (SD) scheme. It consists of two local pulses, but an entangling gate is created when they are applied together. In this chapter, I will discuss how to separate the decoupling gates from the overall evolution of the fixed-coupling system. Therefore, even if implementing a pulse gate takes a long time, it can still be treated as instantaneous.

In section 5.1, I will show that an attempt to implement decoupling based on fast gates applied to the qubits does not work well, due to the coupling terms in the Hamiltonian that do not commute with the gates. In section 5.2, I will introduce a method called separation of the evolution, to implement the decoupling gates. This method has an error of third order in time and I will analyze it in section 5.3. In section 5.4, I will propose a solution to minimize these errors and state that our decoupling method is robust. Finally, in section 5.5, I will show that applying pulse gates after we decoupled the system does not induce extra errors.

## 5.1 Fast Decoupling

One problem of the single-qubit gates in a fixed-coupling multi-qubit system is that the evolution during the gates is perturbed by the coupling terms $H_\text{J}$ in the Hamiltonian. The Hamiltonian of the driven fixed-coupling system is[1]:

$$H(t) = H_\triangle + H_\text{J} + H_\text{ctrl}(t), \tag{5.1}$$

where

$$H_\triangle = -\sum_i \frac{\triangle_i}{2} Z_i, \tag{5.2}$$

$$H_\text{J} = \sum_i J_{i,i+1} X_i X_{i+1} \tag{5.3}$$

and

$$H_\text{ctrl}(t) = \sum_i f_i(t) X_i. \tag{5.4}$$

In the entire Hamiltonian, $f_i(t)$'s are the only controllable parameters, whereas all others cannot be modified freely. In the fixed-coupling regime, all the coupling strengths require to be greater than zero and remain as a constant, which means we need a way to do single-qubit gates while all the couplings are presenting.

One straightforward way to do single-qubit gates is to make the controls as strong as possible and ignore the couplings ($|f_i(t)| \gg J_{i,i+1}, J_{i-1,i}$). This is how NMR decoupling gates work [35] [36].

The superconducting system has the ability to achieve strong qubit-qubit couplings. This is favored comparing to week couplings because the time for an entangling gate to be implemented is upper-bounded by the strength of the relevant couplings. However, in this case the strength of the control pulses $f_i(t)$ may not be much larger. With this limit, the control strengths are generally about twenty times larger than the coupling strengths. The coupling terms in the Hamiltonian is arguably hard to be ignored with this ratio, and most importantly, the error caused by the couplings will be cumulated during rounds of the gate implementations.

A numerical simulation is provided in Fig. 6.3 a). It indicates that twenty single-qubit gate implementations have an overall error about 37.9% if we ignore the couplings, which is unacceptable. Also, the performance will be even worse with more gates applied.[2]

---

[1] The Hamiltonian is pretty much the same as Eq. 4.25, expect we have the extra control term.

[2] All the parameters for the simulation are specified in section 6.3

## 5.2 Slow Decoupling for Free Evolution

A better approach towards implementing the single-qubit gates in the multi-qubit system is more subtle but efficient. I refer this method as the slow pulse gates. This method does not ignore the couplings in a system, but rather regards the coupling terms are evolving alongside of the pulse gates.

The main idea for the slow pulse gates is the Magnus expansion. This expansion provides a way to estimate the evolution of a time-dependent Hamiltonian. Using the expansion, we break the evolution of a system into three evolutions, which are beneficial to our decoupling analysis.

### 5.2.1 Magnus Expansion

An equation of the following form:

$$\frac{dY(t)}{dt} = A(t)Y(t),\tag{5.5}$$

where $A(t)$ and $Y(t)$ are arbitrary time-depedent matrices. The solution of $Y(t)$ can be expressed as a converging Magnus series as long as $\int_{t_i}^{t_f} ||A(t)||dt \leq \pi$ [38]:

$$Y(t_f) = e^{\sum_{k=1}^{\infty} \Omega_k(t_i,t_f)} Y(t_i),\tag{5.6}$$

$$\Omega_1(t_i,t_f) = \int_{t_i}^{t_f} A(t_1)dt_1\tag{5.7}$$

and

$$\Omega_2(t_i,t_f) = \frac{1}{2}\int_{t_i}^{t_f} dt_1 \int_{t_i}^{t_1} dt_2 [A(t_1), A(t_2)].\tag{5.8}$$

For all further terms with $k > 2$, we have the Magnus terms:

$$\Omega_k(t_i,t_f) = O((t_f - t_i)^k).\tag{5.9}$$

For a small $t_f - t_i$, it is quite safe to ignore all the terms with large $k$'s in the expansion, which have higher orders in time, at short times. In our particular case, we are interested in a two-level system, which can be estimated quite well with only the first two terms in the expansion.[38] The main reason is the third order term is about $3 \times 20$ smaller than the second order, where 3 is the constant in the Magnus expansion and 20 is an approximate ratio between control and coupling strengths.

## 5.2.2 Separate the Evolution

In this subsection, I will introduce how to convert from the evolution under a driven fixed-coupling Hamiltonian $H_\triangle + H_J + H_{\text{ctrl}}(t)$ in rotating frame (RF) (defined in 5.1) into two separate evolutions under $H_\triangle + H_J$ and $H_\triangle + H_{\text{ctrl}}(t)$. This analysis is useful because an evolution under $H_{\text{ctrl}}(t)$ can be used to create decoupling gates with 99.99% fidelities.

First, we use the Magnus expansion to express the $|\psi(t)\rangle_{\text{RF}}$ in the Schrödinger's equation (Eq. 5.5), as the following:

$$\frac{d|\psi(t)\rangle_{\text{RF}}}{dt} = -iH_{\text{RF}}(t)|\psi(t)\rangle_{\text{RF}}, \tag{5.10}$$

which gives:

$$|\psi(t)\rangle_{\text{RF}} = e^{\Omega_1(t_i,t_f)+\Omega_2(t_i,t_f)}|\psi(t_0)\rangle_{\text{RF}} + O((t-t_0)^3), \tag{5.11}$$

$$\Omega_1(t_i,t_f) = \int_{t_i}^{t_f} -iH_{\text{RF}}(t_1)dt_1 \tag{5.12}$$

and

$$\Omega_2(t_i,t_f) = -\frac{1}{2}\int_{t_i}^{t_f} dt_1 \int_{t_i}^{t_1} dt_2[H_{\text{RF}}(t_1), H_{\text{RF}}(t_2)]. \tag{5.13}$$

For the clarity of the derivation, we define a new label that will be used throughout this chapter:

$$H_{a[H_b]}(t) \equiv e^{iH_b t}H_a e^{-iH_b t}. \tag{5.14}$$

For the fixed-coupling system that we are interested in (the Hamiltonian is defined in Eq. 5.1), the Magnus terms are:

$$\Omega_1(t_i,t_f) = -i\int_{t_i}^{t_f} dt_1(H_J + H_{\text{ctrl}})_{[H_\triangle]}(t_1) \tag{5.15}$$

$$= -i\int_{t_i}^{t_f} dt_1 H_{J[H_\triangle]}(t_1) - i\int_{t_i}^{t_f} dt_1 H_{\text{ctrl}[H_\triangle]}(t_1) \tag{5.16}$$

and

$$\Omega_2(t_i, t_f) = -\frac{1}{2} \int_{t_i}^{t_f} dt_1 \int_{t_i}^{t_1} dt_2 [H_{\text{ctrl}[H_\triangle]}(t_1), H_{\text{ctrl}[H_\triangle]}(t_2)]$$
$$-\frac{1}{2} \int_{t_i}^{t_f} dt_1 \int_{t_i}^{t_1} dt_2 [H_{\text{J}[H_\triangle]}(t_1), H_{\text{J}[H_\triangle]}(t_2)]$$
$$-\frac{1}{2} \int_{t_i}^{t_f} dt_1 \int_{t_i}^{t_1} dt_2 [H_{\text{J}[H_\triangle]}(t_1), H_{\text{ctrl}[H_\triangle]}(t_2)] + [H_{\text{ctrl}[H_\triangle]}(t_1), H_{\text{J}[H_\triangle]}(t_2)]. \tag{5.17}$$

By rearranging the terms, we can rewrite the system's evolution $U_{\text{tot}}(t_i, t_f)$ as:

$$U_{\text{tot}}(t_i, t_f) = \mathcal{T} e^{-i \int_{t_i}^{t_f} dt H_{\text{RF}}(t)} \tag{5.18}$$
$$= e^{\Omega_1(t_i,t_f) + \Omega_2(t_i,t_f)} + O((t_f - t_i)^3) \tag{5.19}$$
$$= e^{\Omega^J(t_i,t_f) + \Omega^C(t_i,t_f) + h(t_i,t_f)} + O((t_f - t_i)^3), \tag{5.20}$$

where

$$\Omega^J(t_i, t_f) = -i \int_{t_i}^{t_f} dt_1 H_{\text{J}[H_\triangle]}(t_1) - \frac{1}{2} \int_{t_i}^{t_f} dt_1 \int_{t_i}^{t_1} dt_2 [H_{\text{J}[H_\triangle]}(t_1), H_{\text{J}[H_\triangle]}(t_2)], \tag{5.21}$$

$$\Omega^C(t_i, t_f) = -i \int_{t_i}^{t_f} dt_1 H_{\text{ctrl}[H_\triangle]}(t_1) - \frac{1}{2} \int_{t_i}^{t_f} dt_1 \int_{t_i}^{t_1} dt_2 [H_{\text{ctrl}[H_\triangle]}(t_1), H_{\text{ctrl}[H_\triangle]}(t_2)] \tag{5.22}$$

and

$$h(t_i, t_f) = -\frac{1}{2} \int_{t_i}^{t_f} dt_1 \int_{t_i}^{t_1} dt_2 [H_{\text{J}[H_\triangle]}(t_1), H_{\text{ctrl}[H_\triangle]}(t_2)] + [H_{\text{ctrl}[H_\triangle]}(t_1), H_{\text{J}[H_\triangle]}(t_2)]. \tag{5.23}$$

We know that one exponential function can only represent a single evolution, whereas several exponential functions multiplied together can be treated as evolutions performed in a sequence. Here, we use the BCH theorem again to split one exponential function into three with a second order error $g(t_i, t_f)$.

$$e^{\Omega^J(t_i,t_f) + \Omega^C(t_i,t_f) + h(t_i,t_f)} = e^{\Omega^J(t_i,t_f)} e^{\Omega^C(t_i,t_f)} e^{h(t_i,t_f) + g(t_i,t_f)} + O((t_f - t_i)^3)$$
$$= \mathcal{T} e^{-i \int_{t_i}^{t_f} dt H_{\text{J}[H_\triangle]}(t)} \mathcal{T} e^{-i \int_{t_i}^{t_f} dt H_{\text{ctrl}[H_\triangle]}(t)} e^{h(t_i,t_f) + g(t_i,t_f)} + O((t_f - t_i)^3), \tag{5.24}$$
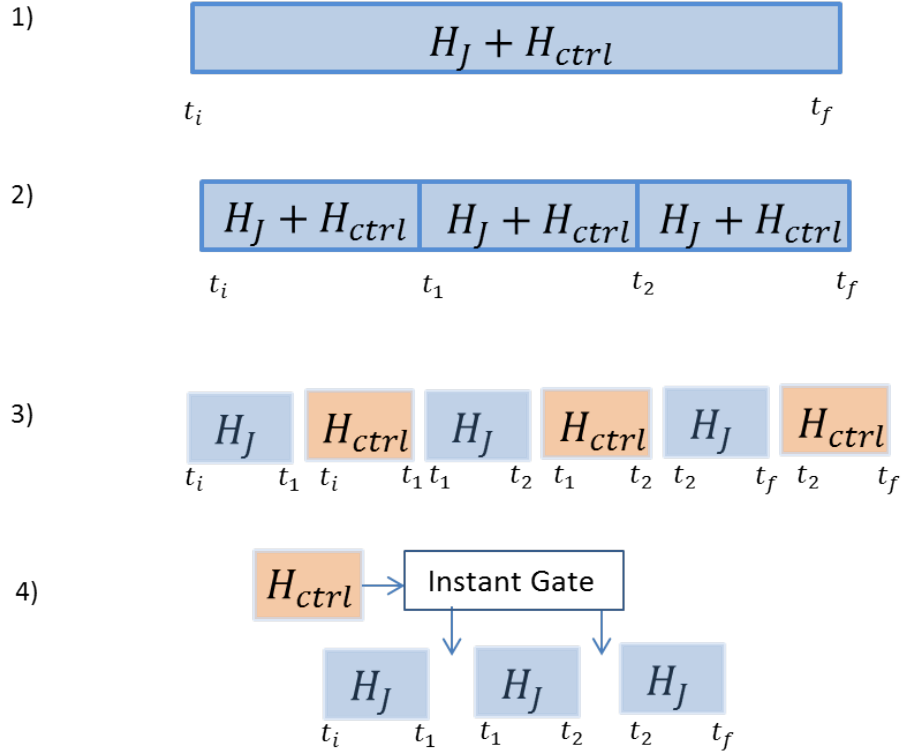
Figure 5.1: **A visualization of steps for estimating the evolution in the rotating frame.** The length of the blocks are associated with the running time of the system, and the heights of the blocks are meaningless. 1) A system evolves from $t_i$ to $t_f$ under the Hamiltonian $H_{\mathrm{J}} + H_{\mathrm{ctrl}}$. 2) The same system can also be seen as three equal time evolutions[4] in a sequence with the same Hamiltonian, where the time intervals are characterized by $t_1$ and $t_2$. 3) Each of the three evolutions can be reformed into evolutions under $H_{\mathrm{ctrl}}$ followed by $H_{\mathrm{J}}$. 4) We can regard the evolutions under $H_{\mathrm{ctrl}}$ as instantaneous gates.

where

$$g(t_i, t_f) = \frac{1}{2}[\Omega^J(t_i, t_f), \Omega^C(t_i, t_f)]. \tag{5.25}$$

Fig. 5.1 gives a vivid cartoon about the process converting from the evolution under the Hamiltonian $H_{\mathrm{J}} + H_{\mathrm{ctrl}}$ to a decoupling sequence. The evolution during a period of time is

---

[4]Three intervals are just for the purpose of the example, the evolution can be segments into any number of intervals.

broken down into evolutions over small time intervals (three as an example in the figure). In each of these small time intervals, the evolution is well approximated by evolving the couplings and controls separately. Since the decoupling gates can be well characterized by the evolutions of the controls, we can assume the evolution during the complete time interval as the couplings with instantaneous decoupling gates.

Note that we have not evaluate the second order (in time) errors in these process yet. The error analysis will be covered in later chapters. For the errors higher than the second order in time, the simulation in Fig. 6.3 shows that they are extremely close to zero. In the figure, the evolution under the Hamiltonian is compared with the separate evolutions of couplings and controls, which we derived using the first two orders in time. It leads to a fidelity of 97.91%, which is very close to the predicted value 97.82%.

## 5.3  Error Analysis

In this section, we will focus on analyzing the total errors during the separation of the evolutions, which are of second order in time. We will derive the exact representation of the error term $E(t_i, t_f)$, which is defined as:

$$E(t_i, t_f) = g(t_i, t_f) + h(t_i, t_f). \tag{5.26}$$

This error term is an overall error, which holds the following equation:

$$\mathcal{T}e^{-i\int_{t_i}^{t_f} dt H_{\mathrm{J}[H_\triangle]}(t) + H_{\mathrm{ctrl}[H_\triangle]}(t)} = \mathcal{T}e^{-i\int_{t_i}^{t_f} dt H_{\mathrm{J}[H_\triangle]}(t)} \mathcal{T}e^{-i\int_{t_i}^{t_f} dt H_{\mathrm{ctrl}[H_\triangle]}(t)} e^{E(t_i, t_f)} + O((t_f - t_i)^3), \tag{5.27}$$

where

$$\begin{aligned} E(t_i, t_f) =& g(t_i, t_f) + h(t_i, t_f) \tag{5.28} \\ =& \frac{1}{2}[\Omega^J(t_i, t_f), \Omega^C(t_i, t_f)] - \frac{1}{2} \int_{t_i}^{t_f} dt_1 \int_{t_i}^{t_1} dt_2 [H_{\mathrm{J}[H_\triangle]}(t_1), H_{\mathrm{ctrl}[H_\triangle]}(t_2)] \tag{5.29} \\ &+ [H_{\mathrm{ctrl}[H_\triangle]}(t_1), H_{\mathrm{J}[H_\triangle]}(t_2)]. \tag{5.30} \end{aligned}$$

We rewrite $g(t_i, t_f)$ as a double integral form[5]:

$$g(t_i, t_f) = \frac{1}{2}[\Omega^J(t_i, t_f), \Omega^C(t_i, t_f)] = \frac{1}{2} \int_{t_i}^{t_f} dt_1 \int_{t_i}^{t_f} dt_2 [H_{\mathrm{ctrl}[H_\triangle]}(t_1), H_{\mathrm{J}[H_\triangle]}(t_2)]. \tag{5.31}$$

Then, we use $g(t_i, t_f)$ to simplify $E(t_i, t_f)$ by combining it with the second term of $h(t_i, t_f)$:

$$\begin{aligned} E(t_i, t_f) =& \frac{1}{2} \int_{t_i}^{t_f} dt_1 \int_{t_1}^{t_f} dt_2 [H_{\mathrm{ctrl}[H_\triangle]}(t_1), H_{\mathrm{J}[H_\triangle]}(t_2)] \\ &- \frac{1}{2} \int_{t_i}^{t_f} dt_1 \int_{t_i}^{t_1} dt_2 [H_{\mathrm{J}[H_\triangle]}(t_1), H_{\mathrm{ctrl}[H_\triangle]}(t_2)]. \end{aligned} \tag{5.32}$$

For the second term in $E(t_i, t_f)$, we change the variable labels $t_1, t_2$ and change the order of the integrals:

$$\begin{aligned} E(t_i, t_f) =& \frac{1}{2} \int_{t_i}^{t_f} dt_1 \int_{t_1}^{t_f} dt_2 [H_{\mathrm{ctrl}[H_\triangle]}(t_1), H_{\mathrm{J}[H_\triangle]}(t_2)] \\ &- \frac{1}{2} \int_{t_i}^{t_f} dt_1 \int_{t_1}^{t_f} dt_2 [H_{\mathrm{J}[H_\triangle]}(t_2), H_{\mathrm{ctrl}[H_\triangle]}(t_1)]. \end{aligned} \tag{5.33}$$

---

[5] Here we take only the first terms of the Magnus coefficients because all other terms give results higher than the second order in time.

Combining the two terms above we find:

$$E(t_i, t_f) = \int_{t_i}^{t_f} dt_1 \int_{t_1}^{t_f} dt_2 [H_{\text{ctrl}[H_\triangle]}(t_1), H_{\text{J}[H_\triangle]}(t_2)]. \tag{5.34}$$

To derive further, we assume $H_{\text{ctrl}[H_\triangle(t)]}$ to be:

$$H_{\text{ctrl}[H_\triangle(t)]} = e^{iH_\triangle t}(\sum_{a=0}^{N} f_a(t)X_a)e^{-iH_\triangle t} \tag{5.35}$$

$$= \sum_{a=0}^{N} f_a(t)(\cos(\triangle_a t)X_a + \sin(\triangle_a t)Y_a), \tag{5.36}$$

where the sum is over the indices $a$ corresponding to the qubits, which we want to drive and $N$ is the total number of qubits.

In a fixed-coupling Hamiltonian, $H_{\text{J}[H_\triangle]}(t)$ is:

$$H_{\text{J}[H_\triangle]}(t) = \sum_{b}^{n-1} J_{b,b+1}(\cos(\triangle_b t)X_b + \sin(\triangle_b t)Y_b)(\cos(\triangle_{b+1} t)X_{b+1} + \sin(\triangle_{b+1} t)Y_{b+1}). \tag{5.37}$$

By substituting $H_{\text{J}[H_\triangle]}(t)$ and $H_{\text{ctrl}[H_\triangle]}(t)$ in Eq. 5.34, we have:

$$E(t_i, t_f) = \int_{t_i}^{t_f} dt_1 \int_{t_1}^{t_f} dt_2 \sum_{a,b}^{N} J_{b,b+1} f_a(t_1)$$

$$[\cos(\triangle_a t_1)X_a + \sin(\triangle_a t_1)Y_a,$$
$$(\cos(\triangle_b t_2)X_b + \sin(\triangle_b t_2)Y_b)(\cos(\triangle_{b+1} t_2)X_{b+1} + \sin(\triangle_{b+1} t_2)Y_{b+1})] \tag{5.38}$$

$$= 2i \sum_{a=1}^{N} \int_{t_i}^{t_f} dt_1 f_a(t_1) Z_a \Big( \sum_{\substack{b=a-1, \\ a+1 \\ b\in[1,N]}} J_{a,b} \int_{t_1}^{t_f} dt_2 \sin\left(\triangle_a(t_2 - t_1)\right) \left(\cos(\triangle_b t)X_b + \sin(\triangle_b t)Y_b\right) \Big). \tag{5.39}$$

The above equation gives an exact expression for the error term. In the next subsection, we will see how to use this expression to make the errors vanish during the evolution of the system.

## 5.4    Effective Error Elimination for the Free Evolution

So far, we see that the evolution of a system is separated into three parts (Eq. 5.27), where one of them being the error term $E(t_i, t_f)$. Since an effective decoupling sequence does not involve the evolution of $E(t_i, t_f)$, it is important to make it zero.

In this section, we show that there are three requirements to fulfill the goal of making $E(t_i, t_f)$ effectively zero. In subsection 5.4.1, I will derive an equation, which describes the fact that error terms can be seen as pairs during the evolution of the system. Using this equation as a guideline, we show that the requirements introduced in subsection 5.4.2, subsection 5.4.3 and subsection 5.4.4 are sufficient conditions for the errors to vanish on the second order of time. To clarify and guide the readers through these subsections, we give here list these three requirements.

**Requirement 1: Decoupling gates have to be applied on non-neighboring qubits.**

We will discuss the non-neighboring gates in subsection 5.4.2. As we mentioned before, a single-qubit (decoupling) gate is implemented through control pulses and the errors are mainly coming from the coupling terms in the Hamiltonian. It turns out that these pulse gates refocus their own errors naturally. However, when we apply another decoupling gate on the nearest qubit, it will interrupts the self-correction process and cause a significant error.

**Requirement 2: Decoupling gates have to be applied frequently.**

The decoupling gates are required to be applied very frequently, which means that a time interval $\delta t$ need to be small, assuming that gates are applied once per each time interval $\delta t$. This requirement is discussed in subsection 5.4.3. According to the Magnus expansion, the errors from separating the evolutions are of the second order and higher in $\delta t$. This means the decoupling gates need to be applied as frequent as possible. Meanwhile, note that the gates are always in pairs, because it takes two single-qubit gates to negate a Hamiltonian (as in Eq. 4.20). As a result, we need an even number of them.

**Requirement 3: The time interval and Zeeman frequencies need to have a proper ratio.**

When doing the decoupling, it is better to choose a time interval $\delta t$ that has the relation of $\delta t = \frac{2\pi m}{\triangle_p}$ for any $m \in I$ and all qubit $p$. This requirement is discussed in subsection 5.4.4. It makes the error term $E(t_{n-1}, t_n)$'s (Eq. 5.39) equal to each other for all integer $n$, so that they will be perfectly refocused over two time intervals.

### 5.4.1  Derivation of Relation between Errors

Recall that in section 5.3 we derived a specific expression for the error term Eq. 5.39. The double integral form has a really complicated solution, and gives little insight of its behavior. In this subsection, I will switch the point of view and derive an equation, which indicates the relation between the error terms and when they are zero.

Recall that the fixed-coupling system evolution $U(0,T)$ in rotating frame (RF) Eq. 2.11 is:

$$U(0,T) = \prod_{n \in even} U(t_n, t_{n+1}) U(t_{n-1}, t_n) \tag{5.40}$$

$$\approx \prod_{n \in even} (e^{\Omega^J(t_n, t_{n+1})} e^{\Omega^C(t_n, t_{n+1})} e^{E(t_n, t_{n+1})})(e^{\Omega^J(t_{n-1}, t_n)} e^{\Omega^C(t_{n-1}, t_n)} e^{E(t_{n-1}, t_n)}), \tag{5.41}$$

where $E(t_{n-1}, t_n)$ is defined in Eq. 5.39; $\Omega^J$ and $\Omega^C$ are defined in Eq. 5.21.

As introduced in section 3.1, $e^{\Omega^C(t_n, t_{n+1})}$ is used to create the $n^{th}$ decoupling gate:

$$e^{\Omega^C(t_n, t_{n+1})} = \mathcal{T} e^{-i \int_{t_n}^{t_{n+1}} dt H_{ctrl}(t)} + O((t_{n+1} - t_n)^3) \equiv \tilde{G}_{n+1} + O((t_{n+1} - t_n)^3). \tag{5.42}$$

So, we can rewrite the evolution as[6]:

$$U(0,T) = \prod_{n \in even} e^{\Omega^J(t_n, t_{n+1})} \tilde{G}_{n+1} e^{E(t_n, t_{n+1})} e^{\Omega^J(t_{n-1}, t_n)} \tilde{G}_n e^{E(t_{n-1}, t_n)}. \tag{5.43}$$

Now, we want to move two error terms together to see if they could cancel. We can switch the coupling evolution with the error term once, because the error is of third order in time:

$$U(0,T) = \prod_{n \in even} e^{\Omega^J(t_n, t_{n+1})} \tilde{G}_{n+1} e^{\Omega^J(t_{n-1}, t_n)} e^{E(t_n, t_{n+1})} \tilde{G}_n e^{E(t_{n-1}, t_n)}. \tag{5.44}$$

The target sequence of the system's evolution is:

$$U_{target}(0,T) = \prod_{n \in even} e^{\Omega^J(t_n, t_{n+1})} \tilde{G}_{n+1} e^{\Omega^J(t_{n-1}, t_n)} \tilde{G}_n. \tag{5.45}$$

By comparing $U(0,T)$ and $U_{target}(0,T)$, we discover that rather than having the error evolutions to be identity, the following condition is sufficient:

$$\tilde{G}_n^\dagger e^{E(t_n, t_{n+1})} \tilde{G}_n e^{E(t_{n-1}, t_n)} = e^{\tilde{G}_n E(t_n, t_{n+1}) \tilde{G}_n} e^{E(t_{n-1}, t_n)} = I, \tag{5.46}$$

---

[6]In the following derivations, we will ignore the third order terms for simplicity.

for all $n \in [1, \frac{T}{\tau} - 1]$, where $\tau = t_n - t_{n-1}$ is a small time interval. Here we use the property of $\tilde{G}_n^\dagger = \tilde{G}_n$ because all $\tilde{G}$'s are of the form Eq. 4.43.

The above equation is all it takes for the decoupling method to be accurate because the errors are getting canceled during the evolution. In the next three subsections, we will find the ways to satisfy this equation.

## 5.4.2 Requirement 1: Non-Nearest-Neighbor Decoupling Gates

The first thing we are going to do to fulfill Eq. 5.46 is by making the following equation to be true:

$$\tilde{G}_n E(t_{n-1}, t_n)\tilde{G}_n = -E(t_{n-1}, t_n) \tag{5.47}$$

for all $n \in I$.

This relation is desired because it provides a way to cancel the errors using two consecutive intervals. By looking at Eq. 5.46, an error term with the negative sign has the potential to cancel the term with the positive sign (if they are equal in magnitude, which we will cover this in subsection 5.4.4) for all pairs of errors.

Recall that the $E(t_{n-1}, t_n)$ and $\tilde{G}_n$ are:

$$E(t_{n-1}, t_n) = \sum_a^N p_a(t_{n-1}, t_n)Z_a X_{a+1} + q_a(t_{n-1}, t_n)Z_a X_{a-1} \tag{5.48}$$

$$+ r_a(t_{n-1}, t_n)Z_a Y_{a+1} + s_a(t_{n-1}, t_n)Z_a Y_{a-1} \tag{5.49}$$

$$\tilde{G}_n = \sum_x \cos(n\triangle_x \delta t)Y_x - \sin(n\triangle_x \delta t)X_x, \tag{5.50}$$

where $p_a(t_{n-1}, t_n), q_a(t_{n-1}, t_n), r_a(t_{n-1}, t_n), s_a(t_{n-1}, t_n)'s$ are some constants result from calculating the double integral over $\delta t = t_n - t_{n-1}$ on all qubit $a$, and $x$ is the index for qubits with the decoupling pulses.

To satisfy this relation, we need the decoupling gates to not applying on any two nearest-neighbor qubits. Assuming a pulse sequence of $\tilde{G}_n$ only applies a pulse on qubit $x$, at a certain time interval $\delta$:

$$\tilde{G}_x = \cos(n\triangle_x \delta)Y_x - \sin(n\triangle_x \delta)X_x. \tag{5.51}$$

This pulse gate will induces an error evolution, where the exponent $E(t_{n-1}, t_n)$ has the form:

$$E(t_{n-1}, t_n) = \sum_{\substack{n=x-1, \\ x+1}} (p_a(t_{n-1}, t_n)X_{a+1} + q_a(t_{n-1}, t_n)X_{a-1} \tag{5.52}$$

$$+ m_a(t_{n-1}, t_n)Y_{a+1} + n_a(t_{n-1}, t_n)Y_{a-1})Z_x, \tag{5.53}$$

where we see that our decoupling gate $\tilde{G}_x$, which is a linear combination of $Y_x$ and $X_x$ will negate this error term. However, if there is another decoupling pulse gate on qubit $x+1$, there will not only be new error terms introduced, but all the original ones cannot be negated completely as well, for example, the terms with $X_{a+1}Z_a$ and $Y_{a+1}Z_a$.

### 5.4.3 Requirement 2: Frequent Decoupling Gates

This condition is very critical for eliminating the errors. Throughout the thesis, we are ignoring the third order terms in the time interval $\delta t$ assuming only one decoupling gate is applied per interval. The evolution of coupling and gates are of the first order in $\delta t$, whereas the $E(t_n, t_{n+1})$ is of the second order.

By having a small time interval, the magnitude of error terms will be suppressed. So that, the decoupling sequence can be predict very precisely. As a result, we need the time interval $\delta t$ to be as small as possible. This means two things, there should be no 'free' time between two decoupling gate implementations and they should be implemented very fast.

### 5.4.4 Requirement 3: Proper Ratios between Zeeman Terms and Time Interval

In this subsection, I will show the conditions to make the error terms $E(t_n, t_{n+1})$ equal to a constant for all $n$.

Building on the Eq. 5.46 and Eq. 5.50, we have:

$$e^{E(t_{n-1}, t_n)} e^{\tilde{G}_{n+1} E(t_n, t_{n+1}) \tilde{G}_{n+1}} = e^{E(t_n, t_{n+1})} e^{-E(t_{n-1}, t_n)}, \tag{5.54}$$

for all possible value of $n$. According to Eq. 5.46, we like the above equation to be identity in order to minimize the errors. This leads to the following condition:

$$I = e^{E(t_n, t_{n+1})} e^{-E(t_{n-1}, t_n)}, \tag{5.55}$$

$$\tag{5.56}$$

where one solution is:

$$E(t_n, t_{n+1}) = E(t_{n-1}, t_n). \tag{5.57}$$

Furthermore, we need this condition over all the possible values of $n$, so that, the most general condition is:

$$E(t_{i-1}, t_i) = C \quad \text{for all } i \in I, \tag{5.58}$$

where $c$ is a time-independent matrix (operator).

There is one easy condition to make sure the decoupling has no second order errors. We can derive it by expressing $E(t_n, t_{n+1})$ in terms of previous time interval $E(t_{n-1}, t_n)$ and the time interval length $\delta t$:

$$E(t_n, t_{n+1}) = E(t_{n-1} + \delta t, t_n + \delta t)$$

$$= \sum_a^N \int_{t_{n-1}+\delta t}^{t_n+\delta t} dt_1 i f_a(t_1) Z_a \Big[ \sum_{\substack{b=a-1, \\ a+1}} \int_{t_1}^{t_n+\delta t} dt_2 \sin\left(\triangle_a(t_2 - t_1)\right) \left(\cos(\triangle_b t_2) X_b + \sin(\triangle_b t_2) Y_b\right) \Big]$$

$$\tag{5.59}$$

$$= \sum_a^N \int_{t_{n-1}}^{t_n} dt_1 i f_a(t_1 + \delta t) Z_a \Big[ \sum_{\substack{b=a-1, \\ a+1}} \int_{t_1}^{t_n} dt_2 \sin\left(\triangle_a(t_2 + \delta t - (t_1 + \delta t))\right)$$

$$\left(\cos(\triangle_b(t_2 + \delta t)) X_b + \sin(\triangle_b(t_2 + \delta t)) Y_b\right) \Big]$$

$$\tag{5.60}$$

$$= \sum_a^N \int_{t_{n-1}}^{t_n} dt_1 i f_a(t_1 + \delta t) Z_a \Big[ \sum_{\substack{b=a-1, \\ a+1}} \int_{t_1}^{t_n} dt_2 \sin(\triangle_a(t_2 - t_1))$$

$$\left(\cos(\triangle_b t_2 + \triangle_b \delta t) X_b + \sin(\triangle_b t_2 + \triangle_b \delta t) Y_b\right) \Big].$$

$$\tag{5.61}$$

Now, we want the above equation to be equal between a finite $\delta t$ and $\delta t = 0$. There are many solutions to it, where an obvious one would be:

$$\triangle_p \delta t = 2\pi m \tag{5.62}$$

$$f_a(t + q\delta t) = f_a, \tag{5.63}$$

for all $p$ in $[0, N]$ and $q, m$ are integers.

## 5.5 Gate Implementation on Decoupled System

Using the decoupling method, we are able to manipulate couplings in a Hamiltonian and only keep the useful ones. In this section, we will see how CNOT gates (which are the actual gates we want to apply in the first place) can be applied to the decoupled system. It turns out that as long as the CNOT gates are not applied on the same qubits as the decoupling gates, we can just apply them without further modifications (details are covered in subsection 5.5.1).

The following steps can be considered as a guideline to implement CNOT in multi-qubit system:

1. In a fixed-coupling superconducting system, we first modify the parameters and choose the time interval $\delta t$ to satisfy the relation $\triangle_p \delta t = 2\pi m$ for all $p$.

2. Then, we construct the decoupling sequence by figuring out what are the couplings needed to be decoupled (details are covered in subsection 5.5.2).

3. In the decoupled system, we can apply the CNOT gates to the desired qubits.


### 5.5.1 CNOT Gates with Decoupled Hamiltonian

The decoupling method we discussed so far has not covered the case where extra pulses (that are not decoupling pulse gates) are involved. In this subsection, I will show that having extra gates in a decoupled system will not affect the quality of the decoupling.

We will start the proof by assuming an extra controlling term $H_{\text{extra}}(t)$ (for example CNOT gate pulses) in the Hamiltonian (Eq. 5.1):

$$H_{\text{RF}}(t) = [H_{\text{J}} + H_{\text{ctrl}}(t) + H_{\text{extra}}(t)]_{H_\triangle(t)}; \tag{5.64}$$

$$H_{\text{extra}}(t) = \sum_c f_c(t) X_c, \tag{5.65}$$

where $H_{\text{extra}}(t)$ has the same form of $H_{\text{ctrl}}(t)$, but it is acting on the qubits involved in the CNOT gates rather than the qubits getting decoupled.

Similar to section 5.2, we can apply the Magnus expansion to the evolution, and separate it into two components. Only this time, $\Omega^J(t_i, t_f)$ contains the extra evolution $H_{\text{extra}}$ as

42

well:

$$
\begin{aligned}
\Omega_{\text{new}}^{J}(t_i, t_f) = & \int_{t_i}^{t_f} dt_1 (H_{\text{J}} + H_{\text{extra}}(t_1))_{[H_\triangle(t_1)]} \\
& + \frac{1}{2} \int_{t_i}^{t_f} dt_1 \int_{t_i}^{t_1} dt_2 [(H_{\text{J}} + H_{\text{extra}}(t_1))_{[H_\triangle(t_1)]}, (H_{\text{J}} + H_{\text{extra}}(t_1))_{[H_\triangle(t_2)]}],
\end{aligned}
\tag{5.66}
$$

which results in a new error function $E_{\text{new}}(t_i, t_f)$ (similar to Eq. 5.28):

$$
E_{\text{new}}(t_i, t_f) = h_{\text{new}}(t_i, t_f) + g_{\text{new}}(t_i, t_f),
\tag{5.67}
$$

where $h_{\text{new}}(t_i, t_f)$ is:

$$
\begin{aligned}
h_{\text{new}}(t_i, t_f) = & \frac{1}{2} \int_{t_i}^{t_f} dt_1 \int_{t_i}^{t_1} dt_2 [(H_{\text{J}} + H_{\text{extra}}(t_1))_{[H_\triangle(t_1)]}, H_{\text{ctrl}}(t_2)_{[H_\triangle(t_2)]}] \\
& + [H_{\text{ctrl}}(t_1)_{[H_\triangle(t_1)]}, (H_{\text{J}} + H_{\text{extra}}(t_2))_{[H_\triangle(t_2)]}].
\end{aligned}
\tag{5.68}
$$

As we will show later in subsection 5.5.2, the pulse CNOT gates are never applied on the same qubit as the decoupling gates, so that their Hamiltonians commute:

$$
[H_{\text{ctrl}}(t_1)_{[H_\triangle(t_1)]}, H_{\text{extra}}(t_2)_{[H_\triangle(t_2)]}] = 0,
\tag{5.69}
$$

which gives back the same error term:

$$
h_{\text{new}}(t_i, t_f) = h(t_i, t_f).
\tag{5.70}
$$

Similarly, the another error term $g_{\text{new}}(t_i, t_f)$ is the same as the old one:

$$
g_{\text{new}}(t_i, t_f) = \frac{1}{2} [\Omega_{\text{new}}^{J}(t_i, t_f), \Omega^C(t_i, t_f)]
\tag{5.71}
$$

$$
= \frac{1}{2} [\Omega^J(t_i, t_f), \Omega^C(t_i, t_f)] + \frac{1}{2} [\int_{t_i}^{t_f} dt_1 H_{\text{extra}}(t_1)_{[H_\triangle(t_1)]}, \Omega^C(t_i, t_f)] + O((t_f - t_i)^3),
\tag{5.72}
$$

where the third term comes from the non-commutativity between $H_{\text{extra}}(t)_{[H_\triangle(t)]}$ and $H_{J[H_\triangle(t)]}$; the second term gives a value of zero because two Hamiltonians are not on the same qubit. As a result, this gives the expression:

$$
g_{\text{new}}(t_i, t_f) = g(t_i, t_f) + O((t_f - t_i)^3).
\tag{5.73}
$$

43

As we can see, further control pulses (gates) implemented on the decoupled system do not cause extra errors. One thing worth mentioning is that none of the decoupling pulses are implemented on the qubits that are expected to remain coupled. This is an useful characteristic that allows us to avoid the problem of having decoupling gates and the CNOT gates on the same qubits.

## 5.5.2  Parallel Implementations

So far, we discussed the topological requirements for the decoupling method in the system with nearest-neighbor couplings, it has two major restrictions:

1. Decoupling gates cannot be applied on the nearest-neighboring qubits.

2. Decoupling gates cannot be applied on the CNOT gate qubits.

The above conditions raise a problem that parallel gates may not be able to carry out in a single run. For example, two CNOT gates in a four-qubit array. Theoretically, they can be implemented at the same time. However, this is not the case for our method because we need some 'free' qubits to apply the decoupling gates. Therefore, we actually need two rounds of gates to do it.
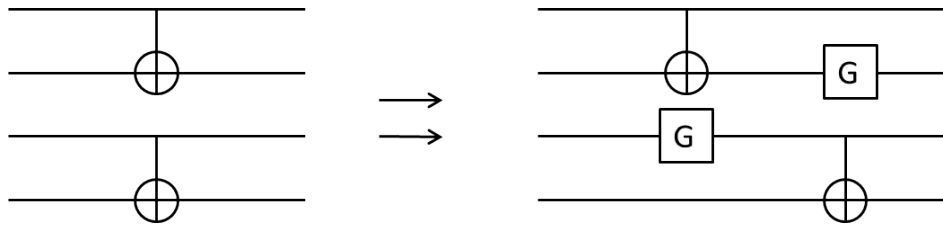


Figure 5.2: **Two parallel CNOT implementations in the four-qubit system.** In order to do two CNOT gates in a fixed-coupling system, we need to decouple the coupling between the qubit 2 and 3. As a result, two CNOT gates need to be implemented through two time-steps. Here, $G$ stands for the frequently applied decoupling gates.

In fact, we are going to prove that for any form of parallel gates with any number of qubits, our decoupling method takes at most four time-steps. In fact, for most of the time, people can figure out themselves how to insert the decoupling gates in their systems. I will demonstrate the structural approach in the following procedures:

### 1. We can ignore all the single-qubit gates in the circuit at first.

First of all, we ignore all the single-qubit gates and reconstruct the circuit with only two-qubit gates. This is because single-qubit gates are rather easy to 'slip' in after we figure out the decoupling sequence. Even in the case that the couplings associate with the single-qubit gates are not decoupled, it only gives a non-scalable error of second order in time.

### 2. We identify the gaps and their parities.

When applying gates in parallel, the qubit without gate implementations is an 'inactive qubit'. We call a chain of such qubits sandwiched by two CNOT gates in the 1D array 'a gap'. For all the gaps in the system, we find their parities (whether the number of the qubits is odd or even). If a gap has an odd number of qubits, we know that applying the decoupling pulses $\tilde{G}$ on alternative qubits is able to decouple all these qubits. If a gap has an even number of qubits, we need to introduce the four-qubit decoupler to decouple these qubits.

### 3. We can implement all the CNOT gates with the help of four-qubit decoupler.

I will refer the sequence of decoupling gates ($\{\tilde{G}_n\}$ discussed in Eq. 4.43) as one-qubit decoupler. A four-qubit decoupler[7] for the 1D-array (shown in Fig. 5.3) consists of two one-qubit decouplers on first and fourth qubits and CNOT applied twice on qubits two and three.

---

[7]It is definitely better to have a two-qubit decoupler and I believe it is achievable, however, we have not delicate our time to this topic yet.
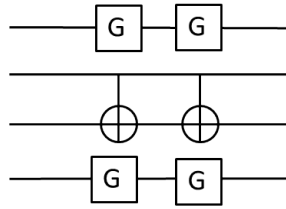
Figure 5.3: **A 4-qubit decoupler.** Two rounds of decouple pulses sandwiched CNOT gates.

This decoupler is useful in two aspects. First of all, it can decouple even qubit gaps. Meanwhile, with at most four time steps, a chain of CNOT gates can be implemented using the four-qubit decouplers shown in Figure 5.4.

**4. At last, we can add back the single-qubit gates.**

Sadly, some single-qubit gates cannot be applied in a decoupled environment. Some of the qubits are already occupied by the decoupling pulses. The way we choose to do a single-qubit gate on an occupied qubit is to replace the last pulse gate in the decoupling sequence $G$ with the gate we try to implement. This will only leads to a small error. Refering back to Fig. 6.3, we see that one single-qubit gate even without decoupling still possess a high fidelity (about 99.93%), as long as we do not stack many of them together.

Figure 5.4: **Implementation of a circuit occupied with CNOTs.** CNOTs are separated into four time steps. Red boxes are four-qubit decouplers; Black $G$ gates are one-qubit decouplers.
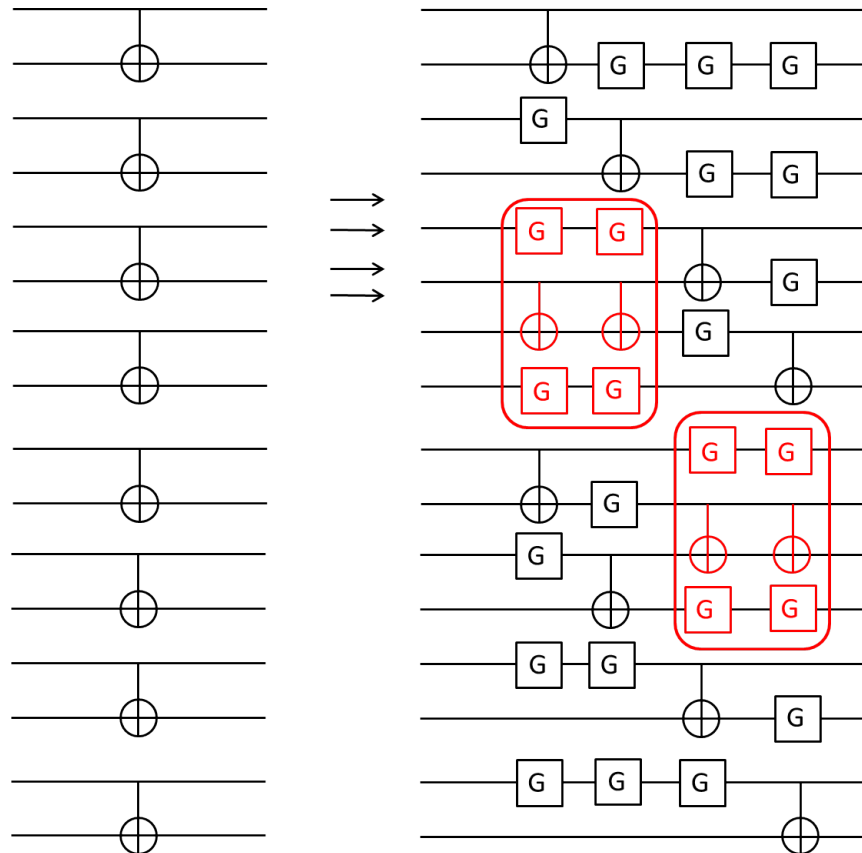
# Chapter 6

# Verification and Visualization

In this chapter, we focus on the numerical simulations of CNOT gates in the multi-qubit 1D-chain fixed-coupling system. We take several steps to achieve this goal, where these steps are covered as sections in this chapter. The first two sections introduce the required background. They introduce the fixed-coupling system itself, the pulse gate performances (without extra couplings) and the metrics we use to measure the system. Next, I will demonstrate the performance of the non-nearest-neighboring decoupling gates in a five-qubit system. In the last section, I will evaluate the performance of the decoupling method by implementing CNOT gates on both three-qubit and five-qubit systems. From the simulations, we will see that our decoupling method successfully suppress the irrelevant couplings.

In more details, the content of this chapter is as follows. In section 6.1, I will give the definitions of fidelity and Schmidt strength, and argue that these two metrics are reasonable and sufficient to serve our purpose of measuring how well a system is being decoupled. In section 6.2, I will introduce the parameters that we use to construct the fixed-coupling system. Also, I will introduce the methods to implement single-qubit and CNOT gates and their fidelities (in the system without extra couplings). In section 6.3, I will discuss the implementation of the decoupling sequence and use it to illustrate the method of refocusing in the five-qubit system. In section 6.4, using the decoupling method we derived in early chapters, I will illustrate the CNOT implementations in multi-qubit system.

## 6.1 Fidelity and Schmidt Strength

In the first part of this section, I will introduce the fidelity function that is used in the simulations. Fidelity is a measurement of how close two gates are, concerning the performance. The fidelity $F$ between $U_1$ and $U_2$ both with dimension $d \otimes d$ is defined as [25]:

$$F(U_1, U_2) = \frac{1}{d^2} |tr(U_1^\dagger U_2)|. \tag{6.1}$$

The fidelity $F(U_1, U_2)$ ranges from 0% to 100%, where 100% means $U_1$ behaves exactly the same as $U_2$ up to a global phase. In this chapter, we drop the variables associate with $F$ since it is always obvious what are the operators being compared.

To serve the purpose of this thesis, we are also interested in how much a group of qubits is entangled with another group, where the degree of entanglement can be characterized by the Schmidt strength. [39] Given an operator $U$ in the tensor produce space and its two subsystems characterized by $P$ and $Q$, each representing a group of qubits. In order to calculate the Schmidt strength between these two groups, we first do the Operator Schmidt Decomposition:

$$U(P, Q) = \sum_i \alpha_i P_i \otimes Q_i, \tag{6.2}$$

where $\alpha_i$'s $> 0$ are Schmidt coefficients and $P_i, Q_i$'s are orthonormal operator bases for system $P$ and $Q$. Based on this decomposition, the Schmidt strength $s(U)$ is defined using the Schmidt coefficients as:

$$s(U) = -\sum_i \alpha_i^2 \log_2(\alpha_i^2). \tag{6.3}$$

As an example, we calculate the Schmidt strength of the CNOT gate expressed in the tensor basis:

$$\text{CNOT} = \frac{1}{\sqrt{2}} |0\rangle\langle 0| \otimes \sqrt{2}I + \frac{1}{\sqrt{2}} |1\rangle\langle 1| \otimes \sqrt{2}X. \tag{6.4}$$

We find that the Schmidt coefficients are $\alpha_1 = \alpha_2 = \frac{1}{\sqrt{2}}$, which gives the Schmidt strength:

$$s(\text{CNOT}) = -\frac{1}{2} \log(\frac{1}{2}) - \frac{1}{2} \log(\frac{1}{2}) = 1. \tag{6.5}$$

For any two-qubit system, the Schmidt strength between two qubits range from 0 to 2. Here, We see that $s(\text{CNOT}) = 1$, which means that the CNOT gate entangles two qubits significantly[1].

---

[1]In fact, a swap gate possess the highest entangling strength of 2, which consists of three CNOT gates.

## 6.2 Simulation Setup

### 6.2.1 Three/Five-Qubit System Setup

We consider an implementation with superconducting qubits. With a CNOT gate of 20 ns and a coherence time of 60 $\mu$s, the gate error, estimated as the ratio between gate time and coherence time, is no more than 0.03%. Therefore, in the regime we consider, errors are dominated by the coherent dynamics.

For a five-qubit system:

$$H_{\mathrm{LF}} = - \sum_{i=1}^{5} \frac{\triangle_i}{2} Z_i + \sum_{j=1}^{4} J_{j,j+1} X_j X_{j+1}, \tag{6.6}$$

the parameters are set to the followings[2]:

$$\triangle_1 = \triangle_3 = \triangle_5 = 2\pi \times 5 \text{ GHz}, \tag{6.7}$$
$$\triangle_2 = \triangle_4 = 2\pi \times 7 \text{ GHz} \tag{6.8}$$

and

$$J_{1,2} = J_{2,3} = J_{3,4} = J_{4,5} = 2\pi \times 100 \text{ MHz}. \tag{6.9}$$

The parameters are set to typical values for experiments. Also, for a three-qubit system, we exclude the qubit 4 and 5. Even though we mentioned in Requirement 3 (Eq. 5.62) that a set of particular Zeeman terms are needed, I find that setting the parameters to arbitrary values give similar performances, even with non-integers. This is a topic worth exploring, but we will settle the argument that the errors cause by not obeying Requirement 3 is small for now, as indicated in the simulations.

Another interesting topic is the cross-talks in the system. In addition to the ideal nearest-neighbor couplings that are assumed in this thesis, there are inevitable long distance couplings in a real experimental implementation. In this thesis, we will ignore the coupling strengths because they are second order in $J_{i,i+1}$. Furthermore, our method can potentially decouple these cross-talks using the Hadamard matrices [35] [36].

---

[2]As we mentioned before, we use the Plank unit in this section as well.

## 6.2.2 Implementation of Single-Qubit Gates on the Isolated Qubit

In this subsection, we discuss the parameters for implementing the single-qubit gate in a single-qubit system. In particular, we want to implement the single-qubit decoupling gate of the form (Eq. 4.43):

$$\tilde{G}(\xi) = \cos(\xi)Y - \sin(\xi)X. \tag{6.10}$$

The parameter $\xi$ depends on the time of the decoupling gate $\tilde{G}(\xi)$ being applied. As we discussed in section 4.3, a qubit can be decoupled from the system by repetitively applying the gate $\tilde{G}(\xi)$ on it[3] (Eq. 4.42). $\xi$ is set to a new value every time: $\xi = \triangle \times t$.

The Hamiltonian[4] of a single qubit is:

$$H_{\text{single}} = -\frac{\triangle}{2}Z + a(t)\cos(\omega t + \psi)X. \tag{6.11}$$

Using the theory covered in section 3.1, we choose the control frequency and phase as:

$$\omega = \triangle \tag{6.12}$$

and

$$\psi = \xi + \frac{\pi}{2}. \tag{6.13}$$

For the case of this single-qubit gate applied in a multi-qubit system, $\omega$ is always matched with the Zeeman frequency of the 'gate qubit'. For the control strength $a(t)$, there is no particular value favored, we choose to analyze the following value:

$$a(t) = 2\pi \times 1.25 \ r(t,T) \ \text{GHz}, \tag{6.14}$$

where $T$ is the total gate time and $r(t,T)$ is the pulse shape function defined as:

$$r(t,T) = \begin{cases} -\frac{1}{2}\cos(\frac{3\pi t}{T}) + \frac{1}{2}, & \text{if } t < \frac{T}{3} \\ 1, & \text{if } \frac{T}{3} \leq t \leq \frac{2T}{3} \\ \frac{1}{2}\cos(\frac{3\pi t}{T} + 4\pi) + \frac{1}{2}, & \text{if } t > \frac{2T}{3} \end{cases} . \tag{6.15}$$

The pulse is shaped to reduce transitions between the Floquet system of the driven system [40]. In order to achieve a high fidelity single-qubit gate, the control pulse needs to be turned on and off slowly and gradually. This leads to the implementation time $T = 0.75$ ns and the fidelity between the pulse implementation and the desired gate Eq. 6.10 is 99.89% on average.

---

[3]We will refer to this set of $\tilde{G}(\xi)$ as the decoupling sequence.
[4]This is the lab frame Hamiltonian. Of course, we use RF for the gates implementation.
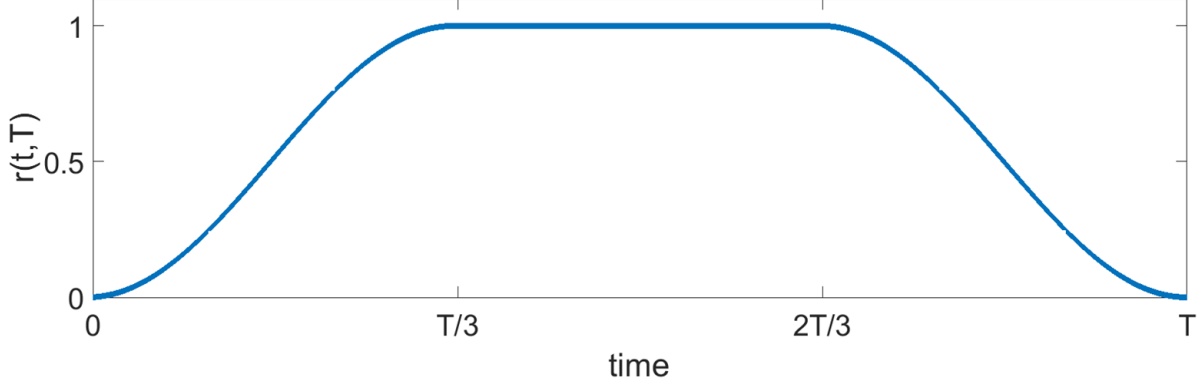
Figure 6.1: **Shape of the Pulse Strength Used in the Single-Qubit Gate Implementation.** For an arbitrary period of time $T$, we plot the behavior of $r(t,T)$ in Eq. 6.15.

### 6.2.3 Implementation of the CNOT Gate on an Isolated Two-Qubit System

In this subsection, a CNOT gate in a two-qubit system is simulated. The goal is to find a proper control pulses for a CNOT gate, so that, we can use it in the decoupled system later.

The two-qubit fixed-coupling Hamiltonian is:

$$H_{\text{two}}(t) = -\frac{\triangle_1}{2}Z_1 - \frac{\triangle_2}{2}Z_2 + a_1(t)\cos(\omega_1 t + \psi_1)X_1 + a_2(t)\cos(\omega_2 t + \psi_2)X_2. \quad (6.16)$$

With the Selective Darkening method introduced in section 3.2, we calculate the following parameters:

$$a_1 = 2\pi \times 0.285 \text{ GHz}, \quad (6.17)$$
$$a_2 = 2\pi \times 0.0166 \text{ GHz}, \quad (6.18)$$
$$\omega_1 = \omega_2 = 2\pi \times 4.9958 \text{ GHz} \quad (6.19)$$

and

$$\psi_1 = \psi_2 = 0. \quad (6.20)$$

The gates have the implementation time $t = 14.84$ ns and the fidelity between the pulse implementation and ideal CNOT gate is 99.6% on average. This number is not optimal, where the main error source is proportional to the strength of the control pulses. We can achieve a better fidelity by applying weaker controls. Even though this leads to longer gate time, but the decoherence error does not increase much.
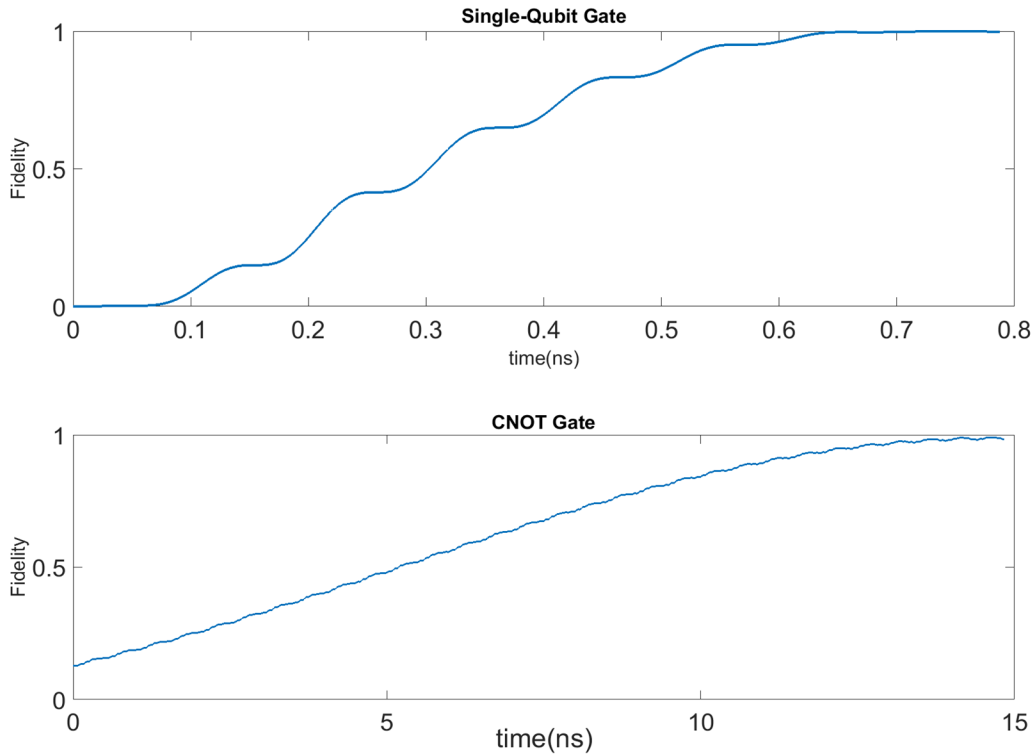


Figure 6.2: **Single and CNOT gate implementations.** The fidelities between the implementation and the ideal gate are plotted. Top: The single-qubit gate implementation has a fidelity of 99.89% at 0.75 ns. Since we are pushing the limit of the strength of the control pulse, we see the Rotating Wave Approximation (RWA) starts to break down[6] resulting the fast oscillations shown in the graph. Bottom: The CNOT gate implementation has the fidelity of 99.6% at 14.84 ns.

---

[6]This breakdown is acceptable, we can still achieve a high fidelity using the technique of pulse shaping. [40]

## 6.3   Refocusing in Five-Qubit System

In this section, we are going to discuss the effectiveness of the fully decoupling (refocusing) method in the five-qubit system. We will show that the five-qubit system without any control pulses evolves away from being identity significantly. Then, we will use the single-qubit pulses to implement the decoupling sequences on qubit 2 and 4 to decouple all the couplings in the system and measures the performance of the system. By comparing two scenarios, there is a clear indication that our decoupling method protects the system from couplings very well.

**Case 1: The Free Evolution Compared with Identity**

Using the numerical simulation in Matlab, we can obtain the evolution of the five-qubit system with the parameters in Eq. 6.14. In the Rotating Frame (RF), the not driven system only evolves under the couplings. We compare the fidelity between the operator that describes the simulated evolution and the identity operator. In Fig. 6.3, we see that the fidelity is 62.09% at 15.2 ns. This indicates that the coupling terms in the five-qubit Hamiltonian influences the evolution significantly. The overall time 15.2 ns corresponds to the CNOT implementation time, which means it is not feasible to ignore the couplings during the CNOT implementation.

**Case 2: The Decoupled Evolution Compared with The Ideal Gates**

In this case, we segment the overall time into twenty intervals. Then, for each interval $a$ we apply the pulses to implement the following gate:

$$\left(\cos(a\triangle_2\tau)Y_2 - \sin(a\triangle_2\tau)X_2\right)\left(\cos(a\triangle_4\tau)Y_4 - \sin(a\triangle_4\tau)X_4\right). \tag{6.21}$$

The control parameters for implementing the above gate is chosen according to subsection 6.2.2. These parameters achieve the gate fidelity of 99.89% in the isolated single-qubit system.

Plotted in Fig. 6.3, we compare the fidelity between the simulated evolution with the ideal gate $T_m$ after the $m$th interval:

$$T_m = \left(\cos(m\triangle_2\tau)Y_2 - \sin(m\triangle_2\tau)X_2\right)\left(\cos(m\triangle_4\tau)Y_4 - \sin(m\triangle_4\tau)X_4\right)T_{m-1} \tag{6.22}$$

and

$$T_0 = I \tag{6.23}$$

for all $m \in [1, 20]$.

We obeserve that the fidelities are always high at each time interval. The overall fidelity is 97.91%, which is extremely close to the fidelity for twenty gates in no extra coupling case which is $99.89\%^{20} = 97.82\%$. Meanwhile, we see that the fidelities from comparing the evolution with the ideal gate after odd number of intervals are slightly lower than the even ones. This is because the couplings are decoupled in pairs as discussed in chapter 4 and for odd intervals the couplings are not decoupled yet.
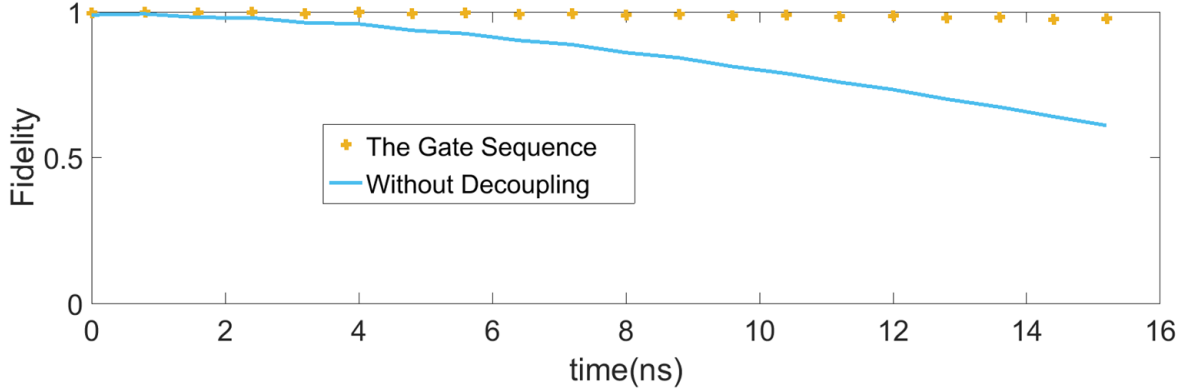


Figure 6.3: **The Five-Qubit System With and Without Decoupling.** The Blue line indicates the fidelity between the free evolution of the five-qubit system without the control pulses and the identity operator. The fidelity decreases with time and the fidelity is 62.09% at $t = 15.2$ ns. Then, we decouple the system by applying the single-qubit pulses as in Eq. 6.21. There are twenty implementations of single-qubit gate for each qubit 2 and 4. The yellow dots indicates the fidelities between the system's evolution under the control pulses and the ideal case stated in Eq. 6.22 after each completion of the single-qubit gate implementation. The overall fidelity (the last yellow point) is 97.91%.

## 6.4 CNOTs implementation in the Three/Five-Qubit System

### 6.4.1 CNOT in Three-Qubit System

In this subsection, we will use the decoupling method to discuss the implementation of a CNOT gate in the three-qubit system. In this system, it is very important to know whether

the control qubit of a CNOT is the first or second qubit because a strong pulse will induce larger entanglements with other qubits. As we addressed in section 3.1, a CNOT gate is implemented through applying a strong pulse on the control qubit, which is about twenty times the strength of the pulse on the target qubit. I will analyze both cases where the qubit 2 is the control qubit, as well as the qubit 1 is the control qubit. I will call them case A and case B as indicated in Figure 6.4.
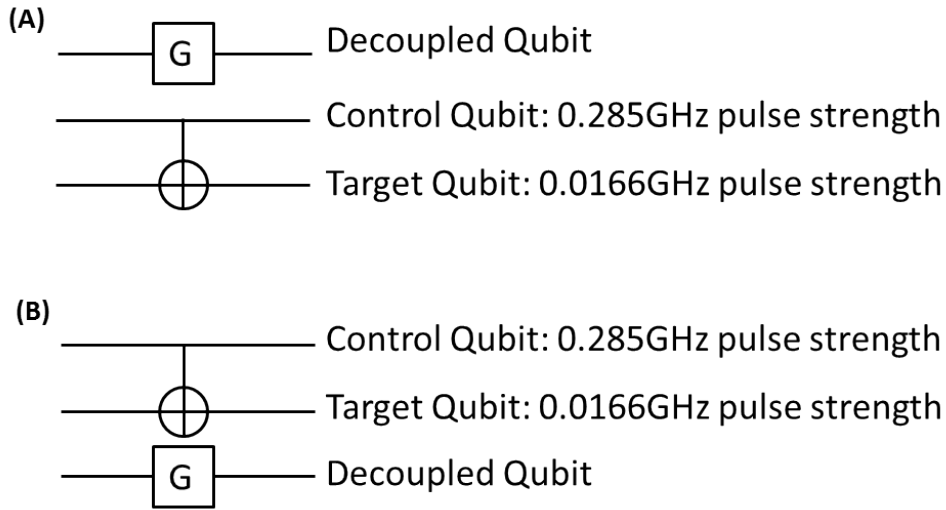


Figure 6.4: **Two different CNOT circuits.** In the case A, two pulses are applied on qubit 2 and 3 to implement CNOT, whereas qubit 1 is decoupled by a decoupling sequence indicated as $G$ in the graph. The pulse amplitudes for each qubit in the pair where the CNOT gate is implemented is taken according to subsection 6.2.3 as indicated on the circuit. For the case B, two pulses (involved in the CNOT implementation) are implemented on qubit 1 and 2, whereas qubit 3 is decoupled.

**Case A:**

For the case A, we decouple the first qubit while implementing the pulses for CNOT on the second and third qubits. The decoupling sequence is defined by the following twenty single-qubit pulse gates:

$$U_D = \prod_{m=1}^{20} \left( \cos(m\triangle_1\tau)Y_1 - \sin(m\triangle_1\tau)X_1 \right), \tag{6.24}$$

56

where $\tau$ is the time interval.

Qubit 2 has a relatively strong control pulse comparing to qubit 1 and 3. The pulse on qubit 3 has a strength reasonably close too zero. Therefore, if there are no decoupling gates applied on the first qubit, the system is controlled almost symmetrically. It means that the control qubit, which induce a CNOT gate on qubit 3, should also induce the CNOT gate on qubit 1. The Schmidt strength between qubits 1&2 should be close to the qubit 2&3, which is also one (Eq. 6.5). However, the Schmidt strength between qubit 1&2 should be zero for the ideal case.



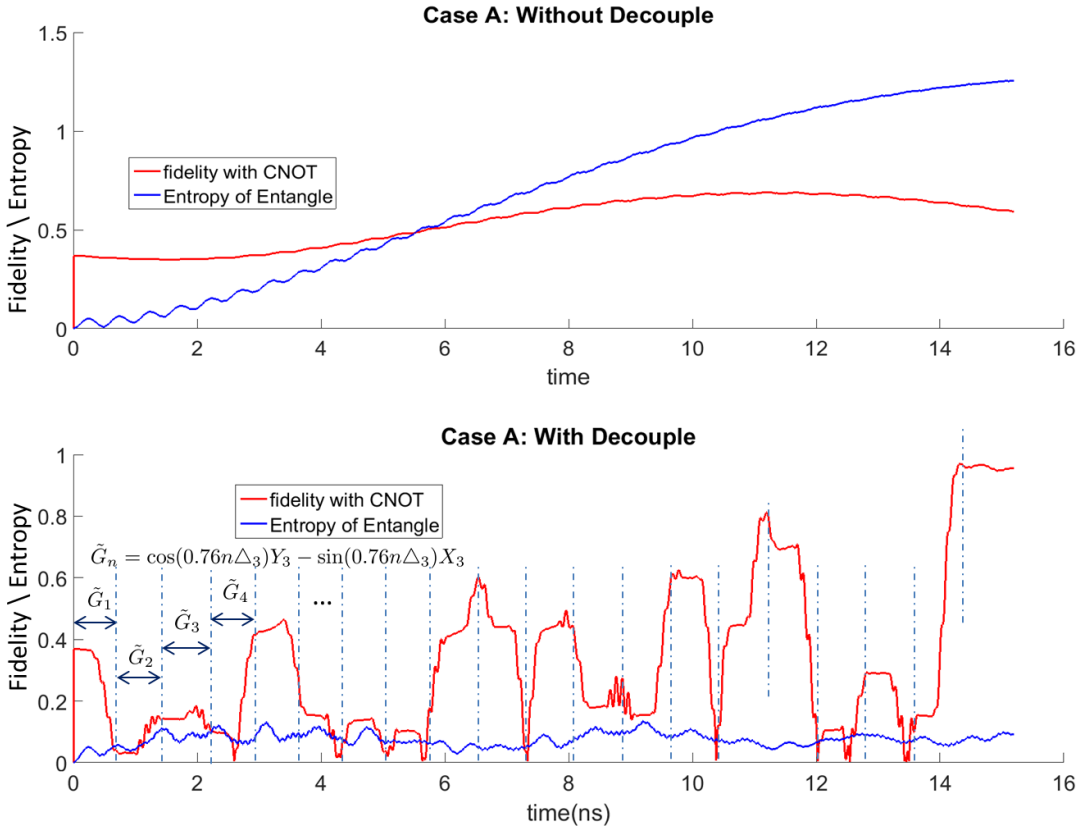Figure 6.5: **Implementations of CNOT gate on the qubit 2 and 3 in the three-qubit system.** Red curves are the fidelities between the evolution of the pulses and ideal CNOT; blue curves are the Schmidt strengths between the qubit 1&2 versus time. Top: An implementation of the CNOT gate without decoupling. Bottom: The CNOT implementation on the qubit 2 and 3 with the qubit 1 decoupled as presented in Fig. 6.4 a.

There are two simulations shown in Fig. 6.5. For the top figure, I apply the control pulses on qubit 2 and 3 using the parameters in Eq. 6.17. There are no pulses applied on the first qubit. The fidelity for each instance comparing to the ideal CNOT gate is plotted using the red curve. For the bottom figure, the same control pulses are applied on qubit 2 and 3 as in the top figure. In addition to that, I apply twenty single-qubit decoupling pulse gates $U_{\mathrm{D}}(t)$ on qubit 1. The reason for having twenty decoupling gates is because this is the maximum even number that can be applied here as mentioned in subsection 5.4.3. The red curve is the fidelity between the evolution of the pulses and the ideal CNOT with expected frame rotations.

If we look at the top figure of Fig. 6.5, which is a CNOT gate implementation in the three-qubit system without decoupling; the blue curve indicates the Schmidt strength between qubit 1 and 2 at $t = 15.2$ ns is about 1.2, which fits our prediction. The red curve indicates the fidelity is about 50% comparing to the ideal CNOT gate at $t = 15.2$ ns. This fidelity cannot be improved very high even if the optimal single-qubit corrections are applied at the end of the evolution because qubit 1&2 are severely entangled. We find the fidelity after the correction is 72.2%.

If we look at the bottom figure, where we use the decoupling method to decouple the first qubit from the rest. The decoupling sequence we use here is $U_{\mathrm{D}}(t)$ as we mentioned before. The reason of the red curve looks not very smooth is because we do not correct for the single-qubit phase during the evolution. If we look at the blue curve, we see that the Schmidt strengths are being suppressed under 0.1 for the entire evolution. This indicates that our decoupling method is doing the job to prevent qubit 1 from entangling with qubit 2. This gives a fidelity of 96.54% when comparing the ideal CNOT gate, and 97.6% when we numerically find the optimal local gate corrections.

**Case B:**

In this case, the control pulses do not change much from the case A. We apply the CNOT pulses on the qubit 1 and 2, whereas decoupling the qubit 3 similar as Eq. 6.24. Shown in Fig. 6.6, the no decoupling case (top figure) has a very low fidelity and the Schmidt strength at $t = 15.2$ ns is about 0.35. Whereas the CNOT gate with the third qubit decoupled (bottom figure), the fidelity is about 96% without single-qubit corrections and the Schmidt strength is about 0.05. The number difference in the Schmidt strength proves once again that our decoupling method works and has the potential for implementing a scalable CNOT with a high fidelity. After applying the local corrections to our CNOT implementation, we find the gate fidelity increases to 99.2%.
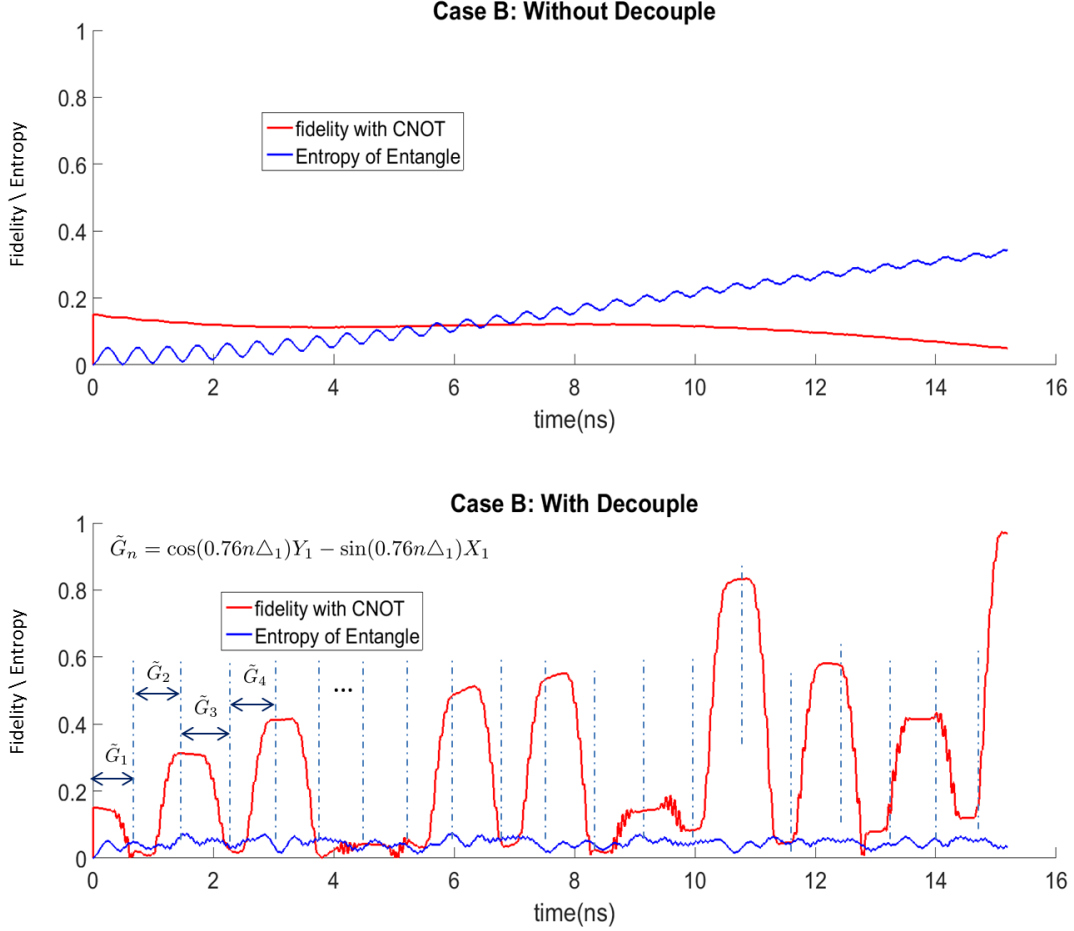
Figure 6.6: **Implementations of CNOT gate on the qubit 1 and 2 in the three-qubit system.** This is very similar to Fig. 6.5. Red curves are the fidelities between the evolution of the pulses and ideal CNOT; blue curves are the Schmidt strengths between the qubit 2&3 versus time. Top: A CNOT gate implementation without decoupling. Bottom: The CNOT implementation on the qubit 1 and 2 with qubit 3 decoupled as presented in Fig. 6.4 b.

Both cases show that our decoupling method is capable of suppressing the couplings between the qubits during the evolution. A weak coupling strength between the CNOT qubits and others indicates that its performance can be further improved through single-qubit gate corrections. We find that in the our decoupled three-qubit system, the CNOT fidelities are 97.6%, 99.2% after we apply the single-qubit gate corrections for case A and

B correspondingly.

## 6.4.2 CNOT in the Five-Qubit System

Besides the three-qubit systems, I also do the simulations of implementing CNOT gates in the five-qubit system described in subsection 6.2.1. It is quite amazing that all of the cases I have done achieve over 92% fidelities without local corrections. I will present some representative ones in this subsection.

The decoupling sequence $U_\mathrm{D}$ is defined similarly as Eq. 6.24:

$$U_\mathrm{D} = \sum_p \left( \prod_{a=1}^{20} \left( \cos(a \triangle_p \tau) Y_p - \sin(a \triangle_p \tau) X_p \right) \right), \qquad (6.25)$$

where the sum is over the indices $p$ corresponding to the qubit $p$ that needs to be decoupled.

Unlike the three-qubit simulations, the phases of each qubit is corrected at every time-step when measuring the fidelities, which means rather than comparing the fidelity with CNOT, we compare the fidelity with $e^{-iH_\triangle t}\mathrm{CNOT}$ at every time $t$. This causes the rapid oscillation of the curve in the graphs. The advantage of plotting the graphs this way is to observe the clear trends with the envelope of the evolutions. We observe that the best fidelities for a) is 92.5% and b) is 93.38%.

Note that the fidelities can be further improved by single-qubit gate corrections as we mentioned before. The fidelity in Fig. 6.7 b) rises from 93.38% to 97.5% with extra local gates applied afterwards (Appendix A.4). Ones may think that this is cheating, however, the fidelity can only be improved by single-qubit gates if the simulated evolution has a similar Schmidt strength with the desired gate; without the decoupling method, single-qubit gate corrections are not able to produce such a high fidelity.

So far, we have seen our decoupling method being applied in the three-qubit and five-qubit systems we specified in section 6.2, where the parameters can be changed within a reasonable range. In section 6.3, we showed that in the five-qubit system, the decoupling pulses can be applied with a very small error. Then in section 6.4, we implemented CNOT gates in both three and five-qubit systems using these decoupling pulses. Even though the threshold of the surface code (99.9%) is not achieved, we argue that the gate fidelities can be further improved to achieve this threshold by having a higher fidelity of the decoupling sequence as well as the CNOT gate we use. The main source of the error in our decoupling method comes from the imperfection of the single-qubit pulse gates we use. Each of them

only has a fidelity of 99.89% in the case of no couplings. Also, the fidelity can be further improved by applying the Gradient Pulse Engineer (GRAPE) to the pulses. On the other hand, we do see that the entanglements between the qubits we want to decouple are being suppressed significantly by the decoupling method we proposed.
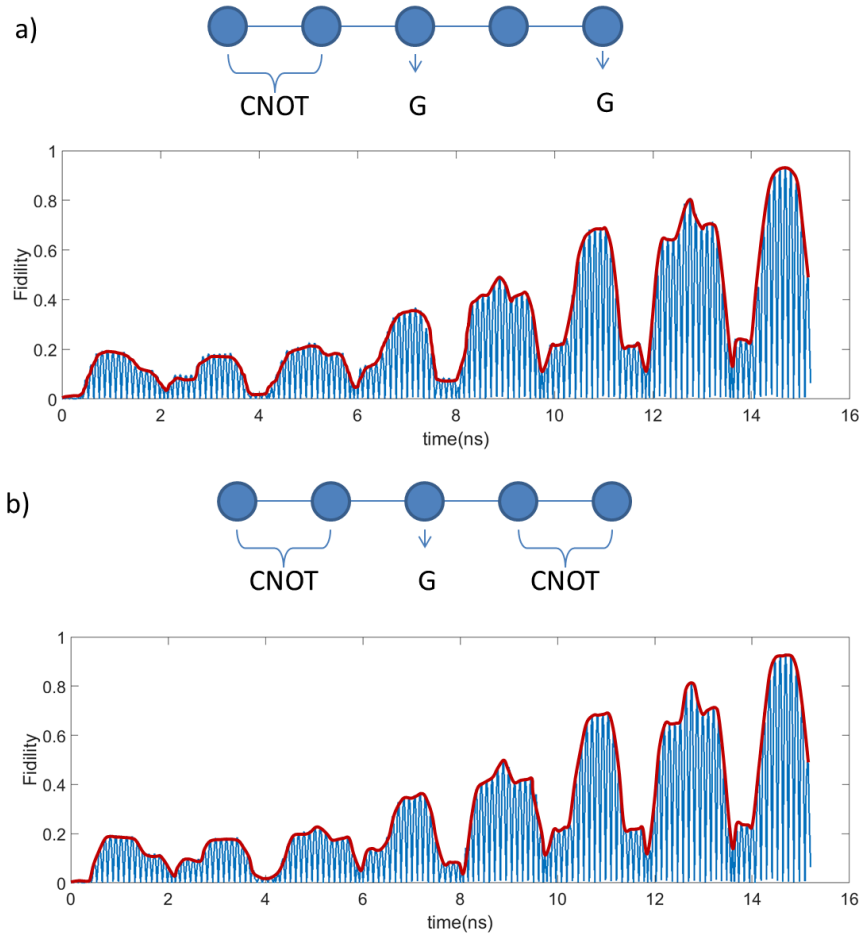
Figure 6.7: **The CNOT gate implementations in the five-qubit system.** a) A CNOT gate is applied on qubit 1 and 2. The qubit 3, 4 and 5 are decoupled by two decoupling sequences $G$. The overall fidelity is 92.5%. b) Two CNOT gates are applied on qubit 1&2 and 4&5 correspondingly. Where qubit 3 is decoupled by a decoupling sequence $G$. The overall fidelity is 93.38%. The blue curves are the fidelities capturing the single-qubit frequencies whereas the red curves represent the evolution in the rotating frame.

# Concluding Summary

In this thesis, we point out the difficulties of a scalable gate implementation in the superconducting system. We argue that a transversed fixed-coupling superconducting system has a long coherence time, but a complicated Hamiltonian. Then, we introduce the superconducting decoupling method that we proposed in this thesis.

The superconducting decoupling method is inspired by the decoupling method in Nuclear Magnetic Resonance (NMR). We make quite a few modifications to the original idea to adapt it in the superconducting system. It transforms a multi-qubit fixed-coupling system into an effective system with only the selected couplings. By manipulating the couplings, we are able to implement one and two-qubit gates to create universal set of gates.

This work still has the potential to be improved and be expanded to more fields. For example, the optical quantum computer has the same form of the Hamiltonians, which means that our method can also be applied. Also, the errors could be further suppressed by higher fidelities on the single-qubit gate implementations we use. This work is also compatible with the GRAPE pulses. It provides an initial state for the GRAPE algorithm to accelerate its running time quadratically.

# References

[1] M. H. Devoret, A. Wallraff, and J. M. Martinis, "Superconducting qubits: A short review," *arXiv preprint cond-mat/0411174*, 2004.

[2] R. P. Feynman, A. R. Hibbs, and D. F. Styer, *Quantum mechanics and path integrals*. Courier Corporation, 2010.

[3] D. Deutsch and R. Jozsa, "Rapid solution of problems by quantum computation," in *Proceedings of the Royal Society of London A: Mathematical, Physical and Engineering Sciences*, vol. 439, pp. 553–558, The Royal Society, 1992.

[4] P. W. Shor, "Polynomial-time algorithms for prime factorization and discrete logarithms on a quantum computer," *SIAM review*, vol. 41, no. 2, pp. 303–332, 1999.

[5] P. Schindler, D. Nigg, T. Monz, J. T. Barreiro, E. Martinez, S. X. Wang, S. Quint, M. F. Brandl, V. Nebendahl, C. F. Roos, *et al.*, "A quantum information processor with trapped ions," *New Journal of Physics*, vol. 15, no. 12, p. 123012, 2013.

[6] T. D. Ladd, F. Jelezko, R. Laflamme, Y. Nakamura, C. Monroe, and J. L. OBrien, "Quantum computers," *Nature*, vol. 464, no. 7285, pp. 45–53, 2010.

[7] D. P. DiVincenzo *et al.*, "The physical implementation of quantum computation," *arXiv preprint quant-ph/0002077*, 2000.

[8] A. Y. Kitaev, "Quantum computations: algorithms and error correction," *Russian Mathematical Surveys*, vol. 52, no. 6, pp. 1191–1249, 1997.

[9] T. Hime, P. Reichardt, B. Plourde, T. Robertson, C.-E. Wu, A. Ustinov, and J. Clarke, "Solid-state qubits with current-controlled coupling," *Science*, vol. 314, no. 5804, pp. 1427–1429, 2006.

[10] A. M. van den Brink, A. Berkley, and M. Yalowsky, "Mediated tunable coupling of flux qubits," *New Journal of Physics*, vol. 7, no. 1, p. 230, 2005.

[11] J. M. Martinis, "Superconducting phase qubits," *Quantum Information Processing*, vol. 8, no. 2, pp. 81–103, 2009.

[12] P. De Groot, S. Ashhab, A. Lupaşcu, L. DiCarlo, F. Nori, C. Harmans, and J. Mooij, "Selective darkening of degenerate transitions for implementing quantum controlled-not gates," *New Journal of Physics*, vol. 14, no. 7, p. 073038, 2012.

[13] C. Rigetti, A. Blais, and M. Devoret, "Protocol for universal gates in optimally biased superconducting qubits," *Physical Review Letters*, vol. 94, no. 24, p. 240502, 2005.

[14] J. M. Chow, A. Córcoles, J. M. Gambetta, C. Rigetti, B. Johnson, J. A. Smolin, J. Rozen, G. A. Keefe, M. B. Rothwell, M. B. Ketchen, *et al.*, "Simple all-microwave entangling gate for fixed-frequency superconducting qubits," *Physical Review Letters*, vol. 107, no. 8, p. 080502, 2011.

[15] N. Khaneja, T. Reiss, C. Kehlet, T. Schulte-Herbrüggen, and S. J. Glaser, "Optimal control of coupled spin dynamics: design of nmr pulse sequences by gradient ascent algorithms," *Journal of magnetic resonance*, vol. 172, no. 2, pp. 296–305, 2005.

[16] D. Lu, K. Li, J. Li, H. Katiyar, A. J. Park, G. Feng, T. Xin, H. Li, G. Long, A. Brodutch, *et al.*, "Towards quantum supremacy: enhancing quantum control by bootstrapping a quantum processor," *arXiv preprint arXiv:1701.01198*, 2017.

[17] E. Lucero, M. Hofheinz, M. Ansmann, R. C. Bialczak, N. Katz, M. Neeley, A. OConnell, H. Wang, A. Cleland, and J. M. Martinis, "High-fidelity gates in a single josephson qubit," *Physical Review Letters*, vol. 100, no. 24, p. 247001, 2008.

[18] P. De Groot, J. Lisenfeld, R. Schouten, S. Ashhab, A. Lupaşcu, C. Harmans, and J. Mooij, "Selective darkening of degenerate transitions demonstrated with two superconducting quantum bits," *Nature Physics*, vol. 6, no. 10, pp. 763–766, 2010.

[19] V. I. Arnol'd, *Mathematical methods of classical mechanics*, vol. 60. Springer Science & Business Media, 2013.

[20] C. Fleming, N. Cummings, C. Anastopoulos, and B. Hu, "The rotating-wave approximation: consistency and applicability from an open quantum system analysis," *Journal of Physics A: Mathematical and Theoretical*, vol. 43, no. 40, p. 405304, 2010.

[21] I. Bloch, "Ultracold quantum gases in optical lattices," *Nature Physics*, vol. 1, no. 1, pp. 23–30, 2005.

[22] R. Ashoori, "Electrons in artificial atoms," *Nature*, vol. 379, no. 6564, p. 413, 1996.

[23] G. Davies and M. Hamer, "Optical studies of the 1.945 ev vibronic band in diamond," in *Proceedings of the Royal Society of London A: Mathematical, Physical and Engineering Sciences*, vol. 348, pp. 285–298, The Royal Society, 1976.

[24] M. A. Nielsen and I. Chuang, "Quantum computation and quantum information," 2002.

[25] A. Gilchrist, N. K. Langford, and M. A. Nielsen, "Distance measures to compare real and ideal quantum processes," *Physical Review A*, vol. 71, no. 6, p. 062310, 2005.

[26] A. Niskanen, K. Harrabi, F. Yoshihara, Y. Nakamura, S. Lloyd, and J. Tsai, "Quantum coherent tunable coupling of superconducting qubits," *Science*, vol. 316, no. 5825, pp. 723–726, 2007.

[27] J. Kelly, R. Barends, A. Fowler, A. Megrant, E. Jeffrey, T. White, D. Sank, J. Mutus, B. Campbell, Y. Chen, *et al.*, "State preservation by repetitive error detection in a superconducting quantum circuit," *Nature*, vol. 519, no. 7541, pp. 66–69, 2015.

[28] L. DiCarlo, J. Chow, J. Gambetta, L. S. Bishop, B. Johnson, D. Schuster, J. Majer, A. Blais, L. Frunzio, S. Girvin, *et al.*, "Demonstration of two-qubit algorithms with a superconducting quantum processor," *Nature*, vol. 460, no. 7252, pp. 240–244, 2009.

[29] C. Rigetti and M. Devoret, "Fully microwave-tunable universal gates in superconducting qubits with linear couplings and fixed transition frequencies," *Physical Review B*, vol. 81, no. 13, p. 134507, 2010.

[30] E. T. Jaynes and F. W. Cummings, "Comparison of quantum and semiclassical radiation theories with application to the beam maser," *Proceedings of the IEEE*, vol. 51, no. 1, pp. 89–109, 1963.

[31] W. Demtröder, *Laser spectroscopy: basic concepts and instrumentation.* Springer Science & Business Media, 2013.

[32] G. W. Johnson and M. L. Lapidus, *Generalized Dyson series, generalized Feynman diagrams, the Feynman integral and Feynman's operational calculus*, vol. 351. American Mathematical Soc., 1986.

[33] P. Benioff, "The computer as a physical system: A microscopic quantum mechanical hamiltonian model of computers as represented by turing machines," *Journal of Statistical Physics*, vol. 22, no. 5, pp. 563–591, 1980.

[34] A. G. Fowler, M. Mariantoni, J. M. Martinis, and A. N. Cleland, "Surface codes: Towards practical large-scale quantum computation," *Physical Review A*, vol. 86, no. 3, p. 032324, 2012.

[35] J. Jones and E. Knill, "Efficient refocusing of one-spin and two-spin interactions for nmr quantum computation," *Journal of Magnetic Resonance*, vol. 141, no. 2, pp. 322–325, 1999.

[36] D. W. Leung, I. L. Chuang, F. Yamaguchi, and Y. Yamamoto, "Efficient implementation of selective recoupling in heteronuclear spin systems using hadamard matrices," *arXiv preprint quant-ph/9904100*, 1999.

[37] J. E. Campbell, "On a law of combination of operators (second paper)," *Proceedings of the London Mathematical Society*, vol. 1, no. 1, pp. 14–32, 1897.

[38] S. Blanes, F. Casas, J. Oteo, and J. Ros, "A pedagogical approach to the magnus expansion," *European Journal of Physics*, vol. 31, no. 4, p. 907, 2010.

[39] S. Balakrishnan and R. Sankaranarayanan, "Measures of operator entanglement of two-qubit gates," *Physical Review A*, vol. 83, no. 6, p. 062320, 2011.

[40] C. Deng, F. Shen, S. Ashhab, and A. Lupascu, "Dynamics of a two-level system under strong driving: Quantum-gate optimization based on floquet theory," *Physical Review A*, vol. 94, no. 3, p. 032323, 2016.

[41] O. Carnal and J. Mlynek, "Young's double-slit experiment with atoms: A simple atom interferometer," *Phys. Rev. Lett.*, vol. 66, pp. 2689–2692, May 1991.

[42] J. Majer, J. Chow, J. Gambetta, J. Koch, B. Johnson, J. Schreier, L. Frunzio, D. Schuster, A. Houck, A. Wallraff, *et al.*, "Coupling superconducting qubits via a cavity bus," *Nature*, vol. 449, no. 7161, pp. 443–447, 2007.

[43] R. Laflamme, E. Knill, D. G. Cory, E. M. Fortunato, T. Havel, C. Miquel, R. Martinez, C. Negrevergne, G. Ortiz, M. A. Pravia, *et al.*, "Introduction to nmr quantum information processing," *arXiv preprint quant-ph/0207172*, 2002.

[44] D. W. Leung, "Towards robust quantum computation," *arXiv preprint cs/0012017*, 2000.

[45] N. Johnston, "QETLAB: A MATLAB toolbox for quantum entanglement, version 0.9." http://qetlab.com, Jan. 2016.

[46] X. Wang, Z. Sun, and Z. Wang, "Operator fidelity susceptibility: an indicator of quantum criticality," *Physical Review A*, vol. 79, no. 1, p. 012105, 2009.

[47] R. R. Ernst, G. Bodenhausen, A. Wokaun, *et al.*, *Principles of nuclear magnetic resonance in one and two dimensions*, vol. 14. Clarendon Press Oxford, 1987.

# APPENDICES

# Appendix A

# Simulation Codes

## A.1   Single qubit Gate

Single qubit gates are simulated with Matlab R2015a.

The following script is used to generate pulse shapes that the applied pulse has rising/falling time:

```
function[y]=pulse_shape_slow(t_total,t)
% This file inputs the total time a pulse
% is intended to run t_total, and the current time t.
% It outputs value y ranging from 0 to 1.

if t < 1/3*t_total
y = -1/2*cos(3*pi*t/t_total)+1/2;
elseif t > 2/3*t_total
y = 1/2*cos(3*pi*t/t_total+4*pi)+1/2;
else
y = 1;
end
```

Then, this script simulates the single-qubit gate of the form $\cos(dt)Y - \sin(dt)X$:

```
function[result]=oneq_mixXY(t_delay,dt)
```

```
% The script takes the input of how long
% the system evolves before we try to implement the gate t_delay
% Also, the value in the decoupling gate dt.
% It produces the fidelity of the pulse gate comparing to the ideal one.

n = 9000;
d = 14*pi;
a = 2.5*pi;
w = -d;
phi = dt+pi/2;
t = 0.75;
x_axis = 0:t/(n-1):t; % x-axis value, the time

%% Operator Define;
X =[0,1;1,0];
Y = [0,-1i;1i,0];
I = [1,0;0,1];
Z = [1,0;0,-1];
G =eye(2);
Expc = [0,-1i*exp(-1i*dt);1i*exp(1i*dt),0]; % Ideal case

for p = 1:n % The recursion
T = p/n*t + t_delay;
H = a*pulse_shape(t,p/n*t)*cos(w*T+phi)*(cos(d*T)*X+sin(d*T)*Y);
E = expm(-1i*(H)*t/n);    %theoretically: phi = phi(de+pi/2)-t_delay*delta
G = E*G;
F(1,p) = 1/2*trace(conj(transpose(G))*Expc);
end
Final = 1/2*trace(conj(transpose(G))*Expc)

%% Plotting Part
result = G;
plot(x_axis,abs(F))
title('Fidelity Compare with Intended gate')
ylabel('Fidelity')
xlabel('time')
```

## A.2 CNOT gate

The script for simulating the CNOT gate is:

```
function[result]=twoq_CNOT(t)
% This script produce a CNOT gate with phases on each state.
% The phase comes from the energy
% pf each state, it is hard to modify.
% The input is the time t we want the pulses to persist
% in the system, and produce the fidelity of the simulated CNOT.
% The overall running time is t = 15.2ns for best fidelity
n = 1800;
x_axis = 0:t/(n-1):t; % x-axis value, the time
d1 = 14*pi;
d2 = 10*pi;
J12 = 0.2*pi;
a1 = 0.57*pi;

%% Operator Define;
X =[0,1;1,0];
Y = [0,-1i;1i,0];
I = [1,0;0,1];
Z = [1,0;0,-1];
X1 = kron(X,I);
X2 = kron(I,X);
Y1 = kron(Y,I);
Y2 = kron(I,Y);
Z1 = kron(Z,I);
Z2 = kron(I,Z);

%% Initiate the parameters
F(:,1) = 0; % Initial fidelity for entangle AF.
theta1 = atan(2*J12/(d1+d2))/2;
theta2 = atan(2*J12/(d1-d2))/2;
a2 = a1*sin(theta1+theta2)/cos(theta2-theta1)
w1 = -d2-J12*(tan(theta1)-tan(theta2))
% the equation from the paper is:
% 0.5*(sqrt(4*J12^2+(d1+d2)^2)-sqrt(4*J12^2+(d1-d2)^2)), they are the same
```

```
w2 = w1;
G = eye(4);

%% entangled states and phased CNOT
Zero = [cos(theta1);0;0;-sin(theta1)];
One = [0;cos(theta2);-sin(theta2);0];
Two = [0;sin(theta2);cos(theta2);0];
Three = [sin(theta1);0;0;cos(theta1)];
Phase_CNOT = [0.4384+0.8933i,0,0,0;0,0.0716+0.9947i,0,0;
              0,0,0,-0.9922-0.0653i;0,0,-0.89-0.4437i,0];

%% The recursion
for p = 1:n
T = p/n*t;
H = J12*(cos(d1*T)*X1+sin(d1*T)*Y1)*(cos(d2*T)*X2+sin(d2*T)*Y2) ...
+a1*cos(w1*T)*(cos(d1*T)*X1+sin(d1*T)*Y1) ...
+a2*cos(w2*T)*(cos(d2*T)*X2+sin(d2*T)*Y2);
E = expm(-1i*(H)*t/n);
G = E*G;
%% With/Without E-initial State
Q(p) = 1/4*trace(transpose(conj(Phase_CNOT))*G);
F(p) = 0.25*(abs(transpose(Zero)*G*Zero)+abs(transpose(One)*G*One)...
            +abs(transpose(Three)*G*Two)+abs(transpose(Two)*G*Three));
end

%% Plotting Part
plot(x_axis,Q)
title('Fidelity Compare with Intended gate')
ylabel('Fidelity')
xlabel('time')
%-------------------------------
%% Some useful parameters
%-------------------------------
F(1,n) %fidelity at final time
G %resulting operator
Gate_time = pi/(2*a1*sin(theta1+theta2)); %theriodical gate time
best_fide_with_change = max(F);
best_fide_without = max(Q);
```

```
Actual_Evo_Matrix = abs(G);
```

# A.3   Three-qubit Gates

QETLAB-0.9 [45] is being used here to find the Operator Schmidt decomposition. The scripts simulate and plot the fidelities as well as the Schmidt strengths.

There are two circuits that I simulated. As I mentioned in Fig. **??**, the first case is CNOT on qubit 1, 2 and decoupling gates on qubit 3.

```
function[]=with_1st_qubit_decouple(t)
% A CNOT pulse applied on three qubit case and has the fidelity of 96.0%.
% t =15.2ns for the best fidelity

%% General Parameters.
n = 5000;
X =[0,1;1,0];
Y = [0,-1i;1i,0];
I = [1,0;0,1];
Z = [1,0;0,-1];
% X gate
X1 = kron(kron(X,I),I);
X2 = kron(kron(I,X),I);
X3 = kron(kron(I,I),X);
% Y gate
Y1 = kron(kron(Y,I),I);
Y2 = kron(kron(I,Y),I);
Y3 = kron(kron(I,I),Y);
% Z gate
Z1 = kron(kron(Z,I),I);
Z2 = kron(kron(I,Z),I);
Z3 = kron(kron(I,I),Z);

%% Underlying system's parameters
d1 = 14*pi;
d2 = 10*pi;
d3 = 14*pi;
```

```
J12 = 0.2*pi;
J23 = 0.2*pi;

a1 = 2.483*pi;
a2 = 0.1;
a3 = 1.7187;
w1 = -d1;
w2 = -31.3794;
w3 = w2;
phi1 = pi/2+d1*t_block;

% axis and expected outcome
x_axis = 0:t/n:t;
evo = eye(8);
Phase_CNOT2 = [0.4488 + 0.8881i,0,0,0;0,0,0,-0.9927 + 0.0018i;
                0,0,0.0835 + 0.9939i,0;0,-0.8445 - 0.5221i,0,0];
Entropy(1) = 0;

% Decouple
t_block = 15.2/20;
t_single = 0.58;

%% Actual evolution of the system
for p=1:n
T = p/n*t;
if mod(p,n/20) == 0
phi1 = phi1+d1*t_block;
end
if mod(T,t_block)>= t_block-t_single
Hrf = J12*(cos(d1*T)*X1+sin(d1*T)*Y1)*(cos(d2*T)*X2+sin(d2*T)*Y2) ...
+J23*(cos(d2*T)*X2+sin(d2*T)*Y2)*(cos(d3*T)*X3+sin(d3*T)*Y3) ...
+0*a1*pulse_shape_slow(t_single,mod(T,t_block)-t_block+t_single) ...
 *cos(w1*T+phi1)*(cos(d1*T)*X1+sin(d1*T)*Y1) ...
+a2*cos(w2*T)*(cos(d2*T)*X2+sin(d2*T)*Y2) ...
+a3*cos(w3*T)*(cos(d3*T)*X3+sin(d3*T)*Y3);
else
Hrf = J12*(cos(d1*T)*X1+sin(d1*T)*Y1)*(cos(d2*T)*X2+sin(d2*T)*Y2) ...
+J23*(cos(d2*T)*X2+sin(d2*T)*Y2)*(cos(d3*T)*X3+sin(d3*T)*Y3) ...
```

```
+a2*cos(w2*T)*(cos(d2*T)*X2+sin(d2*T)*Y2) ...
+a3*cos(w3*T)*(cos(d3*T)*X3+sin(d3*T)*Y3);
end
E = expm(-1i*(Hrf)*t/n);
evo = E* evo;
F2(1,p+1) = 1/8*trace(conj(transpose(        ...
              kron(expm(-1i*d1/2*15.2*Z),Phase_CNOT2)))*evo);

Schdmit_num = OperatorSchmidtDecomposition(evo,[2,4]);
Schdmit_num = Schdmit_num/norm(Schdmit_num);
Entropy(p+1) = 0;
for a = 1: length(Schdmit_num)
Entropy(p+1) = Entropy(p+1) - Schdmit_num(a)^2*log2(Schdmit_num(a)^2);
end
end
F2(1,n+1)
hold on
plot(x_axis,abs(F2(1,:)),'r')
plot(x_axis,Entropy,'b')
hold off
legend('fidelity with CNOT','Entropy of Entangle')
title('Y1 with CNOT23-- No Decouple')
ylabel('Fidelity')
xlabel('time')
```

The second script is similar to first one, but the CNOT is being 'up-side-down'. This put the stronger control pulses near the qubit we want to decouple:

```
function[]=with_3rd_qubit_decouple(t)
% A CNOT pulse applied on three qubit case and has the fidelity of 93.4%.
% The gate time is t=15.2ns
%% General Parameters.
n = 5000;
X =[0,1;1,0];
Y = [0,-1i;1i,0];
I = [1,0;0,1];
Z = [1,0;0,-1];
% X gate
```

76

```matlab
X1 = kron(kron(X,I),I);
X2 = kron(kron(I,X),I);
X3 = kron(kron(I,I),X);

% Y gate
Y1 = kron(kron(Y,I),I);
Y2 = kron(kron(I,Y),I);
Y3 = kron(kron(I,I),Y);
% Z gate
Z1 = kron(kron(Z,I),I);
Z2 = kron(kron(I,Z),I);
Z3 = kron(kron(I,I),Z);

%% Underlying parameter
d1 = 10*pi;
d2 = 14*pi;
d3 = 10*pi;
J12 = 0.2*pi;
J23 = 0.2*pi;

a1 = 0.1;
a2 = 1.7187;
a3 = 2.5*pi;
w1 = -31.3794;
w2 = w1;
w3 = -d3;
phi3 = pi/2+d3*t_block;

% additional
x_axis = 0:t/n:t;
evo = eye(8);
Phase_CNOT2 =  [0.4488 + 0.8881i,0,0,0;0,0,0,-0.9927 + 0.0018i;
                0,0,0.0835 + 0.9939i,0;0,-0.8445 - 0.5221i,0,0];
Entropy(1) = 0;

% Decouple
t_block = 15.2/20;
t_single = 0.58;
```

```
%% Actual evolution of the system
for p=1:n
T = p/n*t;
if mod(p,n/20) == 0
phi3 = phi3+d3*t_block;
end
if mod(T,t_block)>= t_block-t_single && T <= t - t_block
Hrf = J12*(cos(d1*T)*X1+sin(d1*T)*Y1)*(cos(d2*T)*X2+sin(d2*T)*Y2) ...
+J23*(cos(d2*T)*X2+sin(d2*T)*Y2)*(cos(d3*T)*X3+sin(d3*T)*Y3) ...
+0*a3*pulse_shape_slow(t_single,mod(T,t_block)-t_block+t_single) ...
  *cos(w3*T+phi3)*(cos(d3*T)*X3+sin(d3*T)*Y3) ...
+a2*cos(w2*T)*(cos(d2*T)*X2+sin(d2*T)*Y2) ...
+a1*cos(w1*T)*(cos(d1*T)*X1+sin(d1*T)*Y1);
else
Hrf = J12*(cos(d1*T)*X1+sin(d1*T)*Y1)*(cos(d2*T)*X2+sin(d2*T)*Y2) ...
+J23*(cos(d2*T)*X2+sin(d2*T)*Y2)*(cos(d3*T)*X3+sin(d3*T)*Y3) ...
+a2*cos(w2*T)*(cos(d2*T)*X2+sin(d2*T)*Y2) ...
+a1*cos(w1*T)*(cos(d1*T)*X1+sin(d1*T)*Y1);
end
E = expm(-1i*(Hrf)*t/n);
evo = E* evo;
F2(1,p+1) = 1/8* ...
trace(conj(transpose(kron(Phase_CNOT2,expm(1i*d3/2*14.36*Z)))))*evo);

Schdmit_num = OperatorSchmidtDecomposition(evo,[4,2]);
Schdmit_num = Schdmit_num/norm(Schdmit_num);
Entropy(p+1) = 0;
for a = 1: length(Schdmit_num)
Entropy(p+1) = Entropy(p+1) - Schdmit_num(a)^2*log2(Schdmit_num(a)^2);
end
end
evo
hold on
plot(x_axis,abs(F2(1,:)),'r')
plot(x_axis,Entropy,'b')
hold off
legend('fidelity with CNOT','Entropy of Entangle')
```

```
title('CNOT12 with Y3 -- With Decouple')
ylabel('Fidelity')
xlabel('time')

%%%%% how to find the single gate:
%rho = evo
%[s,U,V] = OperatorSchmidtDecomposition(rho,[4,2])
%   --->  s = [2.8149 0.194 0.1799 0.0808]
%This shows that first element is the most important.
%->s1 = 2.8149,
%->U1 =   0.3690 + 0.3338i  -0.0251 - 0.0216i   0.0048 - 0.0090i   0.0238 - 0.0269i
%         0.0281 + 0.0197i  -0.0119 - 0.0438i  -0.0031 + 0.0396i  -0.3057 + 0.3895i
%         0.0084 - 0.0052i   0.0239 - 0.0272i   0.2178 + 0.4467i   0.0082 - 0.0397i
%        -0.0325 + 0.0136i  -0.4653 + 0.1703i  -0.0049 + 0.0370i  -0.0348 - 0.0255i
%->V1 =  -0.7022 - 0.0000i   0.0681 + 0.0482i
%        -0.0660 - 0.0509i  -0.2063 - 0.6712i


%isuni = s(1)*kron(U{1},V{1})
%conj(transpose(isuni))*isuni
%   -> this shows it is 99.0% unitary(we could tell from 2.8149^2/8)

%conj(transpose(V{1}))*V{1} -> [0.5,0;0,0.5]
% This means real_U = U{1}*s(1)/sqrt(2)
% -> abs(real_U) = 0.9903    0.0659    0.0202    0.0715
%                  0.0683    0.0904    0.0791    0.9855
%                  0.0197    0.0720    0.9891    0.0808
%                  0.0702    0.9862    0.0742    0.0858
```

## A.4   Numerical Optimization

I also use Mathematica to numerically find the local gate corrections after we decouple the system to further improve the fidelity, which results in 97.56%:

```
L1 = MatrixExp[I*{{c, a - b*I}, {a + b*I, -c}}];
L2 = MatrixExp[I*{{f, d - e*I}, {d + e*I, -f}}];
L3 = MatrixExp[I*{{C, A - B*I}, {A + B*I, -C}}];
```

```
L4 = MatrixExp[I*{{F, D - Ev*I}, {D + Ev*I, -F}}];
CNOT = {{1, 0, 0, 0}, {0, 0, 0, 1}, {0, 0, 1, 0}, {0, 1, 0, 0}};

P0 = {{0.7380 + 0.6676 I, -0.0502 - 0.0432 I, 0.0096 - 0.0180 I, 0.0476 - 0.0538 I},
{0.0562 + 0.0394 I, -0.0238 - 0.0876 I, -0.0062 + 0.0792 I, -0.6114 + 0.7790 I},
{0.0168 - 0.0104 I, 0.0478 - 0.0544 I, 0.4356 + 0.8934 I, 0.0164 - 0.0794 I},
{-0.0650 + 0.0272 I, -0.9306 + 0.3406 I, -0.0098 + 0.0740 I, -0.0696 - 0.0510 I}};

obj = Tr[KroneckerProduct[L1, L2].P0.KroneckerProduct[L3, L4].CNOT];

Fidelity =
Maximize[{0.25*Norm[obj] , a <= 2*Pi, a >=  0, b <= 2*Pi, b >=  0,
c <= 2*Pi, c >=  0, d <= 2*Pi, d >=  0, e <= 2*Pi, e >=  0,
f <= 2*Pi, f >=  0, A <= 2*Pi, A >=  0, B <= 2*Pi, B >=  0,
C <= 2*Pi, C >=  0, D <= 2*Pi, D >=  0, Ev <= 2*Pi, Ev >=  0,
F <= 2*Pi, F >=  0}, {a, b, c, d, e, f, A, B, C, D, Ev, F}]

=>{0.975766, {a -> 1.02028, b -> 1.41264, c -> 6.28319, d -> 1.29421,
e -> 2.53764, f -> 6.28319, A -> 6.28319, B -> 4.59283,
C -> 5.16391, D -> 0.0485388, Ev -> 3.15469, F -> 1.95426}}
```